

A Parametric Method of Perspective Alignment and Color Correction for Skin Lesion Imaging

A Thesis
presented to
the Faculty of California Polytechnic State University,
San Luis Obispo

In Partial Fulfillment
of the Requirements for the Degree
Master of Science in Industrial Engineering

By

Jian Xu

May 2011

©2011
Jian Xu
ALL RIGHTS RESERVED

COMMITTEE MEMBERSHIP

TITLE: A Parametric Method of Perspective Alignment and Color Correction for Skin Lesion Imaging

AUTHOR: Jian Xu

DATE SUBMITTED: May, 2011

COMMITTEE CHAIR: Dr. Jose Macedo

COMMITTEE MEMBER: Dr. Lily Laiho

COMMITTEE MEMBER: Dr. Lizabeth Schlemer

ABSTRACT

A Parametric Method of Perspective Alignment and Color Correction on Skin Lesion Imaging

Jian Xu

This thesis investigates the employment of a parametric and fiducial-based perspective alignment method, and a color correction method in the context of digital skin lesion imaging. Specifically, the thesis focuses on the problem of restoring geometric and color distortion caused by variable imaging conditions across multiple skin lesion images.

As the first step, an overview of the problem and relevant methods are presented. Next, the theoretical assumptions of relevant methods and practical requirements in clinical environment are compared. Based on the understanding on the goal of the specific medical implementation and characteristics of the relevant methods, we further address the theoretical and practical issues such as the necessity of rigid and parametric methods, using invariant control points as landmarks and inferring the global color variation from the color reference.

The proposed geometric rectification and color correction methods are related with a fiducial mark design which provides control points and color reference for the respective geometric transformation and color calibration.

The experimental results from this thesis show the efficacy of the proposed methods in correcting undesired global geometric and photometric distortion across multiple digital skin lesion images.

Keywords: Skin lesion, digital image registration, perspective alignment, color correction, fiducial mark

ACKNOWLEDGEMENTS

I want to thank my thesis advisor, Dr. Jose Macedo, for encouraging me to focus on the meaningful research and application of medical imaging on skin lesion. I would also like to thank Dr. Lily Laiho and Dr. Lizabeth Schlemer for their contributions and feedback as my thesis committee members. Lastly, I want to thank my parents for their love and support through my time at Cal Poly.

TABLE OF CONTENTS

| | |
|--|------|
| List of Tables | VII |
| List of Figures..... | VIII |
| CHAPTER 1: INTRODUCTION | 1 |
| CHAPTER 2: LITERATURE REVIEW | 3 |
| 2.1 Problem Definition | 3 |
| Engineering of Image Acquisition | 4 |
| Post-processing of the Sensed Images | 5 |
| Geometric Distortion | 6 |
| Color Variation | 7 |
| 2.2 Image Registration | 8 |
| Introduction..... | 8 |
| Geometric Transformation | 11 |
| Projective Transformation | 12 |
| Discussion..... | 14 |
| 2.3 Color Constancy | 15 |
| Introduction | 15 |
| Color Constancy Problem | 18 |
| Algorithms and Assumptions..... | 19 |
| Discussion | 21 |
| CHAPTER 3: METHODOLOGY..... | 23 |
| 3.1 Perspective Alignment..... | 23 |
| Proposed Method | 23 |
| Control Points and Fiducial Design | 25 |
| Experiments and results | 28 |
| 3.2 Color Correction..... | 35 |
| Proposed Method | 35 |
| Context of Skin Lesion Imaging | 35 |
| Color Reference | 38 |

| | |
|--|----|
| Experimental Setting for Image Acquisition | 38 |
| Experimental Design | 41 |
| Performance Metrics. | 42 |
| Image Segmentation | 42 |
| Performance of Color Correction | 44 |
| Result and discussion | 45 |
| CHAPTER 4: CONCLUSION AND FUTURE WORK | 57 |
| Conclusion | 57 |
| Future Work | 58 |
| REFERENCES | 60 |
| Appendix A | 63 |
| Appendix B | 65 |
| Appendix C | 66 |
| Appendix D | 68 |
| Appendix E | 69 |
| Appendix F | 70 |

LIST OF TABLES

| | |
|---|----|
| Table 1 Color difference of skin lesion within the same set of images (Experiment I)..... | 46 |
| Table 2 Color difference of skin lesion within the same set of images (Experiment II)..... | 47 |
| Table 3 Color difference within the same set of images (Experiment III)..... | 48 |
| Table 4 Color difference within the same set of images (Experiment IV) | 49 |
| Table 5 RGB values difference between multiple image sets..... | 50 |
| Table 6 The RGB value of cropped red patch and segmented skin lesion..... | 52 |
| Table 7 Spectral colors and respective ranges of wavelength..... | 55 |

LIST OF FIGURES

| | |
|---|----|
| Figure 1 Geometric distortion..... | 6 |
| Figure 2 Color variation..... | 7 |
| Figure 3 Projective transformation..... | 13 |
| Figure 4 Skin lesion images with perspective variation..... | 14 |
| Figure 5 Fiducial marker..... | 26 |
| Figure 6 Fiducial alignment..... | 26 |
| Figure 7 Perspective alignment by control points..... | 27 |
| Figure 8 Illustration of camera geometry in Experiment I..... | 29 |
| Figure 9 Perspective alignment of a computer graph & print of a standard scene..... | 29 |
| Figure 10 Result of Experiment I..... | 30 |
| Figure 11 Illustration of camera geometry in Experiment II..... | 31 |
| Figure 12 Result of Experiment II..... | 31 |
| Figure 13 Result of Experiment III..... | 32 |
| Figure 14 Variable location of fiducial marker..... | 33 |
| Figure 15 Further registration using McGregor's Method..... | 34 |
| Figure 16 Color correction demonstration..... | 38 |
| Figure 17 Imaging geometry..... | 41 |
| Figure 18 Skin lesion image segmentation..... | 43 |
| Figure 19 R, G and B channel intensity values..... | 44 |
| Figure 20 Color correction result of Experiment I..... | 46 |
| Figure 21 Color correction result of Experiment II..... | 47 |
| Figure 22 Color correction result of Experiment III..... | 48 |
| Figure 23 Color correction result of Experiment IV..... | 49 |
| Figure 24 Color correction result..... | 52 |
| Figure 25 The reflectance spectra of a paper with Fluorescent Whitening Agent | 54 |

CHAPTER 1: INTRODUCTION

The purpose of this thesis is to introduce a parametric method designed to improve the digital skin lesion imaging and its diagnostic accuracy in telemedicine implementation.

The proposed method is designed for restoring perspective variation and color distortion across multiple images of the same scene. The proposed method, algorithms and the design of a rigid fiducial mark are for implementation in the context of skin lesion digital imaging.

During the last few decades, medical imaging has been an essential tool for improving clinical diagnosis and facilitating medical research. Over the past 20 years, the advent of digital image sensor, commercialization of digital camera and availability of internet provide both a new medical imaging method and easier access into telemedicine implementation [1]. Due to the features of digital imaging, it can help dermatologists in monitoring skin lesion progression and the therapeutic efficacy of treatment [1] [2] [3]. There is a large amount of research in skin lesion image acquisition, segmentation, and registration. But the most challenging problem is maintaining a constant scale, perspective and uniform color on the sensed digital lesion image while the camera perspective and the illumination may change. However, research in above topic mainly focuses on image acquisition for providing a constant environment when the scene is photographed. The few automatic and generic algorithms for projective transformation and color constancy do not estimate restoration parameters from invariant features, hence the outcomes lack accuracy and are often unpredictable.

A parametric method is researched for restoring the sensed digital images into a uniform perspective and scale on the same skin lesion area using projective transformation and registration by control points. The research also approached the color constancy problem in skin lesion imaging by providing color calibration using white color information from a color reference and adjusting the intensity values

accordingly. A fiducial mark design incorporating control points and white color reference is introduced for experimental testing. In this thesis, the focus will be skin lesion imaging, though the author notes that the algorithms proposed can be applied in a straightforward way to problems in other domains.

The introduction, categorization, and comparison of different geometric transformations and image registration methods are introduced in Chapter 2 Section 1 where related concepts and terminologies are presented.

The color constancy problem and related correction methods are introduced in Chapter 2 Section 2. Three common and popular color calibration approaches are presented. The comparisons among the assumptions and performances are discussed.

The proposed perspective alignment method and a fiducial design are presented in Chapter 3 Section 1, where detailed transformation type, function, and fiducial features are introduced. In Section 2, the techniques of color calibration and color reference are explained.

Next, the experimental results of the proposed perspective alignment and color calibration methods are presented with quantification analysis.

The last chapter discusses possible improvements to the implementation of the proposed methods, summarizes the lessons learned from this study.

The use of control points in restoring perspective distortion in skin lesion imaging is effective and efficient. The use of fiducial white surface in restoring color variation from exposure and illumination variation is robust under the same type of illumination. The experiments using the designed fiducial mark show that the suggested parametric method and relevant algorithms can be used and further tested under normal field and clinical environment.

CHAPTER 2: LITERATURE REVIEW

2.1 Problem Definition

Image registration is the process of establishing spatial correspondence across two or more images. Over the past few decades, various image registration methods enabled the extraction of quantitative information from a series of images taken under various conditions [1] [5] [6]. In medical imaging application, many registration methods are proposed for their specific medical requirements. In the case of skin lesion screening, digital imaging is widely used by medical professionals for its accuracy, reproducibility and quantification in the way it records pathological skin images.

For the medical process of skin lesion screening, the extraction and quantification of pathological progression features are essential for further evaluation and diagnosis. The essential quantification of progression features is mainly through comparison across two or more images of the same skin lesion taken over time [3] [5] [6] [7] [8].

However, in the image acquisition process, variable imaging conditions often cause unavoidable distortion to the skin lesion features in the sensed images. The existence of geometric and color distortion in the sensed images disturbs the quantification of genuine lesion tissue progression and tends to lower the accuracy of the subsequent medical evaluation.

In medical imaging, there are two common methodologies to reduce or correct undesired effects caused by the variability of imaging conditions.

- Engineering the image acquisition process: engineering equipment , environment and the object during imaging process
- Post-processing the sensed image to correct for the distortion

Engineering of Image Acquisition

The first method, engineering the image acquisition process is common for many photographic and medical imaging processes [1] [7]; for example, engineering of camera settings, illumination, and poses of a model in a studio; engineering the sensor perspective and body poses during an X-ray or MRI (Magnetic Resonance Imaging) process [7].

However, according to some surveys of current dermatological techniques and relevant clinical environments, the image acquisition of skin lesion is not well engineered. For the telemedicine purposes, the users of the imaging device may not be able to engineer the imaging conditions at a professional level. Besides, engineering the imaging process remains a challenging topic for professional photographers, and more or less, undesired variation still exists under engineered solutions.

Given the statistics of pathological skin tissue progression, there may be only subtle change on the region of interest over time, and small variation caused by imaging conditions make it possible to disturb and/or mislead the medical assessment.

In conclusion, engineering the image acquisition is helpful in reducing variation caused by variable imaging conditions. However, it is inappropriate to solely base the reliability of imaging process and reproducibility of lesion images on this manner.

The method proposed in this thesis mainly relies on post-processing to compensate for the variation. However, a small amount of engineering on illumination and camera geometry is suggested for experimental purposes so that the pathological features of skin lesion can at least be preserved in raw image data.

Post-processing of the Sensed Images

The unavoidable variation of imaging conditions over time determines the need of post-processing the sensed images to improve the reliability and accuracy of the following medical assessment and diagnosis.

In the context of skin lesion imaging, the variable imaging conditions often cause two types of distortion across two or more images taken over time. Type I: geometric distortion; Type II: color distortion. The Type I geometric distortion is the target problem for image registration, and will be discussed further in section 1. The Type II color distortion will be discussed in Section 2.

It is worth mentioning that though the same variable factor, for example, camera perspective towards skin lesion may be a common cause to both geometric and color distortion, the resulted distortions should be categorized and different post-processing measures will be used.

One way of rectifying skin lesion images is to have medical professionals manipulate the images with respect to a standard image and/or professional experience. However, human vision lacks accuracy, reproducibility and quantification in the ways it processes geometric and color information. It is difficult for naked eyes to distinguish and precisely quantify distortion and genuine pathological progression.

In the past decades, numerous automatic registration methods have been proposed. With the help of digital sensors, the registration can be done automatically by the computer.

For both manual and automatic skin imaging process, a common problem is a lack of rigid reference to infer the distortion. Unlike the application in brain MRI and bone X-ray, which has rigid features like skull and bones, a standard for deformable skin lesion is rare due to the lack of rigid feature as reference.

Therefore, a rigid reference providing invariant features is necessary for reliable geometric rectification and color calibration in both manual and automatic manner.

Geometric Distortion

In the case of skin lesion imaging, the geometric distortion is often caused by sensor perspective and positioning of the skin lesion of interest [1] [7]. In the sensed images, the effect of geometric distortion between a sensed image (target image) and a reference image is often a geometric variation which complicates the comparison of the pathological features over time and the quantification of local variation caused by genuine tissue progression.

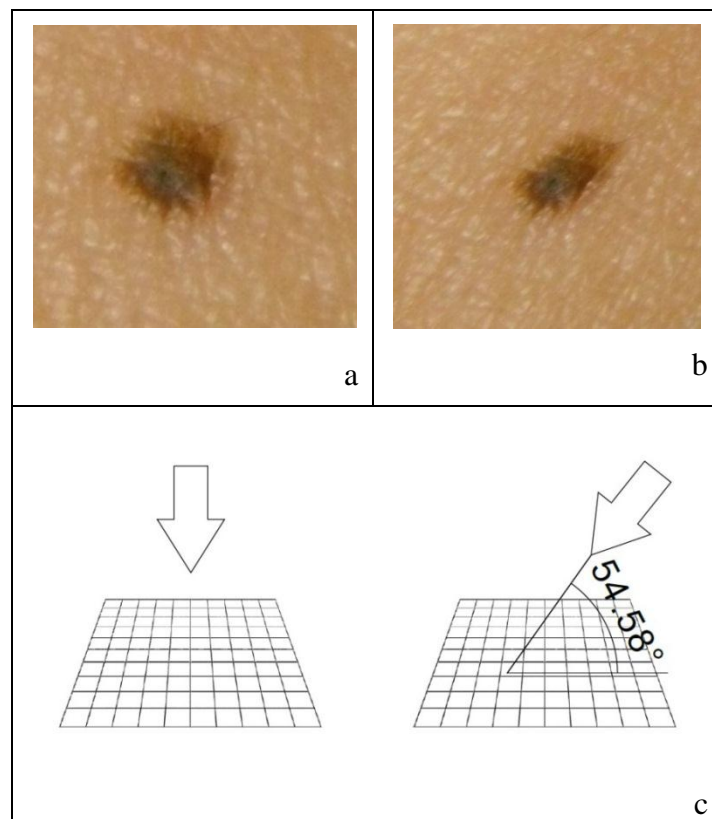


Figure1: Geometric distortion

- a: the reference image of a skin lesion with perpendicular perspective
- b: the sensed image (target image) of the same skin lesion with perspective variation of angle large than 45°
- c: the camera perspective illustration of image a and b

An example of typical geometric distortions on skin lesion images can be seen in Figure 1, which shows a reference image with perpendicular perspective and a geometrically distorted version of the image. It can be observed that the distorted image differs from the reference image in terms of location, perspective, and scale.

This makes it difficult to compare skin lesion images acquired at different times and/or with different imaging conditions for medical diagnosis. Therefore, the geometric rectification of distorted images is necessary for better information consistency and diagnostic accuracy.

Factors that may contribute to the geometric distortion include: camera geometry, three-dimensional features of the skin, pose difference and muscle/skin deformation [1] [2] [3]. The variation is geometric change on the skin area of interest.

The proposed method mainly focuses on the perspective variation across multiple images which are caused by both camera geometry and pose difference. The detailed approach and its performance will be discussed in Chapter 3.

Color Variation

In the case of skin lesion imaging, the color variation is often caused by variable illumination conditions, perspectives, sensor exposures and color imaging setting [1] [10] [11]. In the sensed images, the effect of the color variation between a sensed image and a reference image often exists on the whole region of interest which complicates the comparison of the pathological features over time and the quantification of local color variation caused by genuine tissue progression [1] [2] [3].

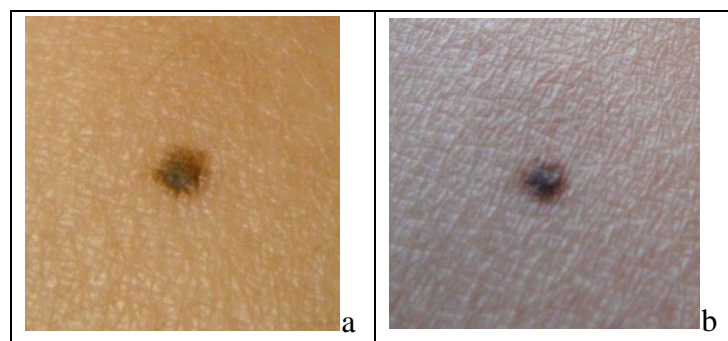


Figure2: Color variation

a: skin lesion image taken under fluorescent light

b: the image of the same skin lesion taken under lateral natural light illumination

An example of typical color distortions on skin lesion images can be seen in Figure 2, which shows two images of the same skin lesion. The left image was taken

under fluorescent light and the other taken under daylight. It can be observed that the second image differs from the first image in terms of brightness, exposure, and color cast. This makes it difficult to compare skin lesion images acquired under different illuminations for medical diagnosis. Therefore, color calibration on one or more images is necessary for better color constancy across multiple images taken over time.

Factor that may contribute to the color distortion includes: imaging geometry, camera response, illumination effect, difference of skin surface reflectance and skin tone change over time.

The proposed method is for compensating the color variation caused by imaging geometry, camera response and illumination effect. The detailed approach will be discussed in Chapter 3.

2.2 Image Registration

Introduction

Given the previous discussion, variation of imaging conditions is unavoidable. After the image was taken, post-processing is necessary to rectify the geometric distortion. Image registration is widely used in medical imaging for the rectification of geometric distortion under either manual or automatic manner.

The categorization of image registration methods is introduced below. Given the characteristics of some image registration categories, many of the affiliated registration methods are not applicable due to the practical condition and the consequent theoretical assumption in skin lesion imaging. Hence, general categorization of the methods will be briefly introduced first and applicable methods will be further discussed in the following sections [1] [5] [6].

Categorization of Image Registration Methods

From the application, image registration methods can be classified based on several criteria [1] [5] [6] [7]. The classifications presented here are partially based on the introduction and categorization of image registration methods of relevant survey papers [I. Maglogiannis, S. Pavlopoulos, & D. Koutsouris, (2004)] [B. Zitova & J.

Flusser, 2003] [J. B. Antoine Maintz & Max A. Viergever 1998] and medical imaging handbook [Ed. Sonka and Milan (2000)].

Some primary subdivisions are:

- **Modality:** Mono-modality refers to the case where all images are obtained by the same imaging sensor type and there are no major differences between the intensity ranges and image manifestations that correspond to the same scene or object. In multi-modality, these ranges can differ drastically and can give distinct manifestations in the sensed images.
- **Dimensionality:** This refers to the number of dimensions of the images. Images have typically been two spatial dimensions. However, several imaging technologies provide 3D volume information. Most of today's applications involve 2D/2D and 3D/3D registration.
- **Subject:** In medical implementation, intra-subject refers to the issue that all images are of the same subject (patient), and typically the same pathological feature of interest. Inter-subject denotes the fact that more than one subject is involved, for example: register two images of two different skin lesions.
- **Nature of Distortion:** Geometric distortion can be attributed to several characteristics, including variable perspective of sensors, temporal changes (e.g. the registration of images of the same skin lesion with pathological progression) and inherent differences (e.g. images of different skin lesions).

From the methodology point of view, registration algorithms can be classified based on several criteria:

- **Information Content:** In the registration context, there are two trends in the type of information acquisition. The Landmark based approaches rely on the existence and detection of landmarks. Geometric alignment is calculated based on these landmarks (points, lines or contours) only. These landmarks usually have clear physical features (e.g. the skull in the case of brain MRI, fiducial markers visible in all modalities.), or they can be of theoretical interest only (e.g. lines, corners, points of high curvature.). In landmark-based registration, performance of the algorithm heavily depends on the

landmark identification. Image content-based approaches, on the other hand, rely on pixel intensity value information. These typically extract features from pixels and calculate an alignment based on the intensity value. They are usually slower than landmark-based algorithms, but have the potential to produce accurate and robust results in contexts when no reliable landmark is found.

- Transformation: Generally speaking, there are two types of geometric transformations: parametric models, e.g. rigid-body, affine, spline based, when a few parameters determine the transformation and nonparametric models (also known as optical flow, dense matching.), when each pixel is allowed to move independently. Note that in the latter case, if there was no restriction on the transformation, an image could be made to look similar to any other image with the same intensity range as the first image. Thus, these methods require regularization to overcome variable pose and incorporate prior knowledge about the deformation field.

Some concepts like similarity measure and optimization are out of the scope of this thesis. In this thesis, the proposed image registration method is two-dimensional, parametric, and fiducial-based. The similarity measure and optimization are not essential for this method.

Image registration is the process of aligning two or more images in order to map the pixel-by-pixel correspondence among a set of images [5]. In other words, given two images which the first is called the reference image and the second the sensed image, the goal of image registration is to find the set of coefficients of a transformation function that map the sensed image to the reference image. This technique is used in a various scientific applications to provide a correspondent view of the image information. In the medical implementation, image registration is used in clinical tasks such as X-ray, MRI, telemedicine and image-guided surgery.

One form of image registration is rigid registration which mainly deals with image alignment. This is in contrast to elastic registration which can compensate for changes in local morphological development over time. In this thesis, the focus is 2-D rigid image registration which the objective of the registration procedure is to find a transformation to apply to the source image that best aligns it with the target image.

Geometric Transformation

Affine transformations: an affine transformation is a mapping from one vector space to another, consisting of a linear part, expressed as a matrix multiplication, and an additive part, an offset or translation. For two-dimensional spaces, an affine transformation [2] [3] [14] is expressed below:

$$[x \ y] = [w \ z] \begin{bmatrix} a_{11} & a_{12} \\ a_{21} & a_{22} \end{bmatrix} + [b_1 \ b_2] \quad (1)$$

where $[w \ z]$ is the point coordinates of an input plane and $[x \ y]$ is the corresponding coordinates in an output plane. For mathematical and computational convenience, the above expression can be written as a single matrix multiplication by adding a third coordinate as:

$$[x \ y \ 1] = [w \ z \ 1] \begin{bmatrix} a_{11} & a_{12} & 0 \\ a_{21} & a_{22} & 0 \\ b_1 & b_2 & 1 \end{bmatrix} \quad (2)$$

note for above two-dimensional affine transformation, the auxiliary third dimension is constant which make the transformation in two-dimensional space.

$$\text{Or } [x \ y \ 1] = [w \ z \ 1]T \quad (3)$$

where T above is called an affine matrix

Common affine transformations include Identity, Scaling, Rotation, Shearing, Reflection and Translation.

Forward mapping

It scans the pixels of the input image and, at each location of input image, (w, z) computing the spatial location, (x, y) , of the corresponding pixel in the output image using the transformation function directly.

$$(x, y) = T(w, z) \quad (4)$$
$$[x \ y \ 1] = [w \ z \ 1]T$$

Inverse mapping

It scans the output pixel locations and, at each location, (w, z) , computes the corresponding location in the input image (x, y) using

$$(w, z) = T^{-1}(x, y) \quad (5)$$
$$[w \ z \ 1] = [x \ y \ 1]T$$

In Figure 3, from the left condition to the right condition, the mapping is usually called forward mapping. On the contrary, it is inverse mapping.

Projective transformation

Another transformation type relevant to the thesis focus is the projective transformations. The previously mentioned affine transformations are a subset of projective transformations. Projective transformations are useful in reversing perspective distortion in an image [14].

Two-dimensional projective transformation expression:

$$[x' \ y' \ h] = [w \ z \ 1] \begin{bmatrix} a_{11} & a_{12} & a_{13} \\ a_{21} & a_{22} & a_{23} \\ b_1 & b_2 & 1 \end{bmatrix} \quad (6)$$

Note that in the auxiliary third dimension, a_{13} and a_{23} are nonzero, and the $x = x'/h$ and $y = y'/h$. Due to the auxiliary non-constant third coordinate h , in a projective

transformation, lines map to lines but most parallel relationships are not kept.

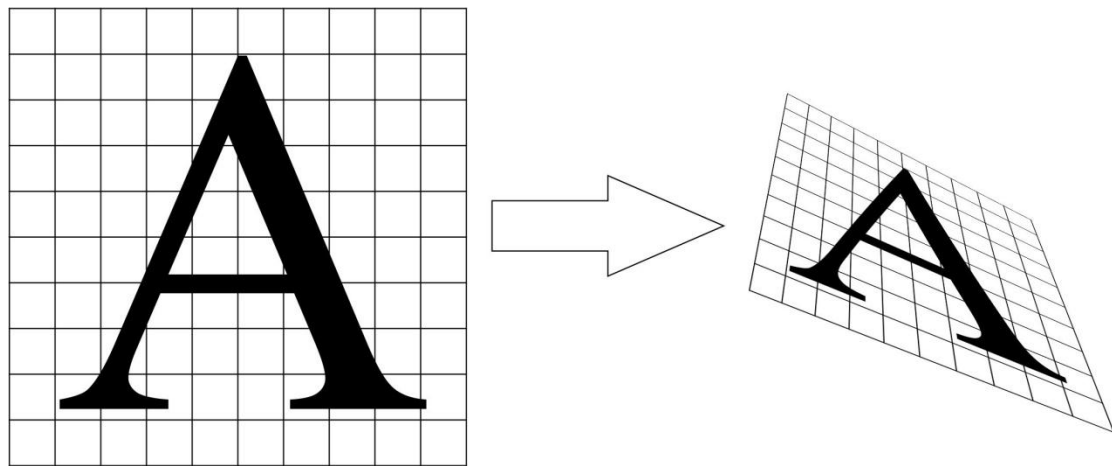


Figure3: Projective transformation

Left: the planar surface with reference image “A” from perpendicular perspective

Right: the planar surface with reference image “A” from non-perpendicular perspective

As shown in above figures, geometric transformations of images are defined in terms of geometric coordinate transformations.

In the case of dermatological diagnosis, the perspective variation is an undesired distortion in the sensed images, and the goal of the perspective alignment is to correct the distortion on the whole image. The local pathological progression on the skin lesion is essential and should be kept for the medical assessment.

From Figure4, given the same perpendicular perspective in the left and middle images, the pathological progression is easy to be detected. The perspective variation and different scaling factor in the right image complicate the detection and quantification of tissue progression. Hence, the goal of the perspective alignment is to restore multiple images into a uniform perspective and scaling that may benefit the medical assessment.



Figure4: Skin lesion images with perspective variation

Left: skin lesion image taken under perpendicular perspective as the reference image

Middle: a synthetic tissue growth, the skin lesion is the same as the sensed image on the right but from the same perspective as the reference image.

Right: a hypothetical sensed image of the same skin lesion taken with a different perspective, and scaling

Discussion

One of the most important applications of geometric transformations is image registration. In medical imaging, image registration is often used to align two or more images of the same scene. In the case of skin lesion imaging, what medical professionals need is the quantification of tissue progression. The unavoidable camera perspective variation towards the region of interest causes confounding geometric misalignment on the whole scene. This misalignment needs to be corrected before any reliable assessment on the skin lesion images. The misalignment from the accurate alignment can be described by a geometric transformation function. With the inverse of the function, the misaligned pixels input can be transformed into correct locations output at the corrected image. Image registration generally consists of four basic steps [5] [6] [7] [14]:

- Feature detection
- Corresponding features matching
- Geometric transformation calculation
- Aligning one image with the others by the geometric transformation

Above four steps will be further discussed in Chapter 3.

2.3 Color Constancy

Introduction

In skin lesion imaging, the quantification and assessment of the color feature on the lesion is often essential for skin cancer diagnosis. In telemedicine or follow up study on skin lesion, it is important that the recorded colors remain similar under a variety of imaging and illumination conditions [1]. In existing research regarding skin lesion imaging in diagnostic context, I. Maglogiannis, S.Pavlopoulos, et al. (2005) proposed a method of engineering image acquisition process for generating reproducible digital images. However, given the practical situation in telemedicine, and clinical environment in dermatology, a constant imaging and illumination condition does not always hold. Hence, when using digital images for skin cancer diagnosis, post-processing of color image is necessary to remove the unavoidable distracting effects caused by imaging and/or illumination factors. This problem is commonly referred to as color constancy, i.e., the constancy of surface color appearance under varying illumination.

When a digital camera captures an image of a scene, the sensor response at each pixel depends on the illumination [10] [11] [12]. Namely, each pixel value of the sensed digital image is related to the color temperature of the light source. A white object usually reflects the effect of illuminant color cast caused by its corresponding color temperature. For example: a piece of white paper will appear reddish under a low color temperature and appear bluish under a high color temperature. Given the task of color correction in sensed digital image, white balance and a variety of other color constancy methods are widely used in the field. The goal of the color correction, in the context of skin lesion imaging, is to process the image so that all skin lesion images look as taken the same canonical illumination [10] [11]. With the least or zero amount of color variation from illuminant color, the genuine color change over time caused by pathological progression can be quantified and assessed by medical

professionals[1][2][3]. Given a scenario of real-time video telemedicine, a constant skin surface color under variable perspective and illumination can convey more reliable diagnostic imaging.

Approaches to color constancy can be sorted into two types [10] [16] [24]. For the first type, the goal is to represent images by features that are independent to the illumination, such as image retrieval. For these types of approaches, the estimation of the light source is not necessary. For the second group, the goal is to correct image color for deviations from a canonical illumination (standard illumination). For these types of approaches, it is necessary to estimate the illumination when the image is taken. Then a recovery of the image color can be done for its estimated description of the scene under a canonical illumination. In this section, the focus is the second type of approach, i.e. approaches rely on estimating illumination for color correction.

Obtaining color constancy is of importance in various applications, and a number of approaches have been proposed to estimate the illumination, Gray World approach; White Patch approach; the gamut mapping approaches; color-by-correlation; neural network approaches[10] [11] [12] [24] [25]. Most of them are based upon certain assumptions of color distribution in the scene and/or in the image and they differ in the way the illumination is estimated.

The gamut mapping approaches; color-by-correlation; neural network approaches are considered most successful ones. Although these three approaches and their derivatives can achieve reasonable levels of color constancy, main drawbacks are also obvious: complexity, requiring image data with known illumination or training of the neural network. All of them rely on the fact that the set of possible colors seen under a canonical illumination is known. That is the base for knowing how any surface in the scene will appear in the sensed image given the known illumination. Furthermore, given the complexity of these algorithms, the unavoidable errors from color correction are often unpredictable and cannot be spotted by human vision which causes artifacts offering erroneous information.

In short, the accuracy of above three methods is based upon a large amount of known information about reflectance and illumination which reduces their scope of

implementation [10] [11] [12] [13]. Given the focus of skin lesion imaging, it may be difficult or even impossible to have a database of skin surface reflectance, illumination, and camera characteristics. Besides, the skin-tone, surface reflectance, and skin lesion color are all variables to be measured and presumably change over time, which makes the matching of the illumination with its estimated color less accurate or even misleading in color correction.

Given the context of skin lesion imaging, the focus of this section is studying less complex and more practical color constancy approaches under real-world limitations. In the field of photography and image processing, white balance and gray balance are two widely used and accepted methods. White Patch and Grey World with their roots in many white/gray balance algorithms are usually considered less complex and low level color constancy algorithms. White-patch approach assumes that the brightest patch of the object in the sensed image is white. Max-RGB estimates the illuminant color from the maximum response of the different color channels. The estimation of illuminant color is based on the color of the brightest patch in the image. Grey-world hypothesis assumes that the average reflectance in the scene is achromatic. The average color of the scene in the image is gray. Hence, any deviation from the measured average corresponds to the effect from illuminant color.

In this section, the effort mainly focuses on low level methods. Each approach is briefly introduced and analyzed within skin lesion imaging context. Then, a fiducial marker with white patch is proposed as white color reference for illuminant estimation. The algorithm of the proposed approach is close to White-Patch and max-RGB, but with a man-made white patch as a more stable reference.

Finally, all three approached are tested using the same set of image data. The color correction results are evaluated by both subjective and objective measures.

Color Constancy Problem

The theoretical image values $f(x)$ for a Lambertian surface depend on the illuminant spectra $e(\lambda)$, the surface reflectance $s(x, \lambda)$ and camera response function $c(\lambda)$, where λ is the wavelength of the light and x is the spatial coordinate [9] [10] [11]:

$$f(x) = \int e(\lambda) s(x, \lambda) c(\lambda) d\lambda, \quad (7)$$

assuming that the scene is illuminated by one illuminant and that the observed color of the illuminant spectra s depends on the spectra of the illuminant source $e(\lambda)$ and the camera response function $c(\lambda)$ then the solution to the estimation of e is:

$$e = \int e(\lambda) c(\lambda) d\lambda \quad (8)$$

given the sensed image values s , both $e(\lambda)$ and $c(\lambda)$ are unknown. The problem of estimating illuminant color is under-constrained, and the goal of color constancy is unattainable without further assumptions.

Algorithms and Assumptions

The following is an overview of the linear color constancy approaches and respective assumptions which they are based upon. Linear color constancy approaches are based on Von Kries hypothesis [18] and his related diagonal model of separate scaling on R, G, and B channels [13]. Von Kries's diagonal model suggests when the frequency responses of R, G, and B components are narrow band and without overlapping on each other, the error of correction through diagonal model is much smaller than that of other illumination estimations [13][18].

Approaches relying on specific illumination properties and/or learning/training methodologies are excluded for their lack of generality and simplicity. RGB color space is chosen in this thesis because of two reasons: it is the most common color space used in digital sensor, display device and image processing software; the processing of RGB values in linear approaches is straightforward and does not require any transformation. Most methods in the paper are applicable to other color spaces, but a comparison across different color spaces is beyond the scope of the current research.

Most low level color constancy methods consist of two steps: they first estimate the effect of illumination, then use the resulted information to compensate for the illuminant color cast in the image.

In photography and image processing, the widely accepted white balance and gray balance methods have similar assumptions and algorithms as those of below methods [10] [11] [24] [25]: White Patch approach, Max-RGB approach and Grey World approach.

A. White Patch approach

The underlying assumption of white patch approach is that the brightest patch in the image is white. The chromaticity of the illuminant is the chromaticity of the white patch. Any shift from the white color inferred from the white patch corresponds to the illuminant color. If half the value of the maximum intensity of 8unit RGB image is defined as the reflectance white (255,255,255). All pixels in an image data are corrected through the following normalization:

$$R_g [i,j] = R[i,j] \times 255 / \max R$$

$$G_g [i,j] = G[i,j] \times 255 / \max G \quad (9)$$

$$B_g [i,j] = B[i,j] \times 255 / \max B$$

where (R_g, G_g, B_g) is the corrected color.

Hsu et al. [10] used a version of white patch approach for color correction. The R, G and B components of the image are adjusted such that the average color value of this reference white patch is grey.

B. Max-RGB Approach

The White-Patch algorithm assumes that the maximum response in an image is caused by a perfect reflectance (i.e. a white patch, see figure to the right). In practice, this assumption is alleviated by considering the color channels separately, resulting in the max-RGB algorithm.

The algorithm is the same as the above; however, max R, G and B values are considered separately, and not necessarily located on the same pixel or same object in the sensed image.

C. Grey-World Approach

Grey-World hypothesis is firstly proposed by Buchsbaum [9] that assumes the average reflectance in a scene is achromatic, given sufficient color variations in the scene [13]. The average reflectance color of the objects in the image is then grey. Any shifts from the measured averages correspond to the illuminant color. If half the value

of the maximum intensity of 8unit RGB image is defined as the reflectance grey (128,128,128). All pixels in an image data are corrected through the following normalization:

$$\begin{aligned} R_g[i, j] &= R[i, j] \times 128/\text{Mean}(R) \\ G_g[i, j] &= G[i, j] \times 128/\text{Mean}(G) \\ B_g[i, j] &= B[i, j] \times 128/\text{Mean}(B) \end{aligned} \quad (10)$$

where (R ,G ,B)is the original color, and (R_g , G_g , B_g) is the corrected color

The Gray World algorithm is widely used because of its simplicity. However, it tends to deviate from ground-truth when its assumption does not hold, namely when the scene has uniform color and its average value deviates from grey (RGB value 128, 128, 128).

Discussion

Given the principles of White-Patch and MaxRGB, the estimation of the illuminant color relies on locating the highest intensity values at the same or different pixel. However, the surface of the physical object in the scene, at the same location, is not necessary to be a true white point. Glossiness of the surface, a single bad pixel or spurious noise will all lead to the incorrect maximum value; hence jeopardize the illuminant estimation [12]. Brian Funt, et al. suggested that above factors are fundamental cause of the poor performance of the MaxRGB and pre-processing is necessary to filter out the noise.

However, in the field, there are more reliable methods to infer the illumination. In photography, a white color surface or a white card is often used as reference to illumination and exposure before or when the image is taken. In the post-processing, the sensed white reference is also commonly used to compensate for the exposure and color cast. If the assumption of uniform illumination and planar surface of the scene are met, a man-made white reference with a determined reflectance is supposed to be the brightest patch in the scene and the sensed image. Hence, illuminant estimation is

more reliable based on above man-made white reference.

The Grey-World approach and its revised versions also suffer from their fundamental assumption that the average intensities of R, G, and B channel of an image data should be equal. There are many situations that the assumption does not stand. For example, most of the time, the skin tone is not likely to give equal average intensities of the three channels.

CHAPTER 3 METHODOLOGY

3.1 Perspective Alignment

As discussed in Chapter 2, the features on the skin surface are deformable hence cannot provide high accuracy for perspective alignment. A rigid fiducial marker with invariant control points is presented in following sections which provide six control points for calculating the parameters of perspective transformation function.

Proposed Method

Assumptions:

Modeling of imaging conditions involves generalization of many causes of variation and exclusion of some rare but extreme situations. This experiment for this thesis makes some simplifying assumptions in order to appropriately test the performance of the proposed method. Many of the assumptions are based on both theoretical and practical conditions. The below assumptions narrow the case in which these results can be held true.

- The geometric misalignment is mainly caused by camera perspectives and body poses. The undesired perspective variation exists on the whole captured skin lesion image. The local deformation on the skin is negligible.
- The skin of interest is considered flat with no obvious three-dimensional characteristics. Such case is to be avoided: the skin on the knees, and finger joints that are highly deformable and may present unpredictable three-dimensional deformation.
- The camera perspective variation across different images should not cause loss of geometric and color features on the region of interest.
- The illumination is uniform on the skin area of interest in one image with no local illumination difference. Such case is to be avoided: part of the image is shadowed; part of the image is highly illuminated.

- Proper exposure is suggested. Although most existing and the proposed color calibration methods can correct for the exposure, extreme overexposure and underexposure can cause loss of tissue features on the skin area. For example, a skin area with RGB values (255,255,255) can be interpreted as an overexposed area since no real skin is that bright under adequate exposure. The diagnostic feature is considered lost since the valuable pixel-wise relationship cannot be restored given all maximum RGB intensity values.

Projective Transformation

Given the assumptions in previous section, and the features of camera perspective variation, projective transformation is chosen as the transformation type to describe and compensate for the geometric variation.

A projective transform keeps straight lines straight but does not preserve the angles between lines. This form of transformation cannot be described by a linear affine transformation, and in fact differs by x- and y-dependent terms in the denominator:

$$\begin{aligned}x' &= (a*x + b*y + c)/(g*x + h*y + 1) \\y' &= (d*x + e*y + f) / (g*x + h*y + 1)\end{aligned}\quad (11)$$

It takes four points, or eight coefficients, to describe this transformation. The projective transform can equivalently be described by a (transposed) matrix equation:

$$\begin{aligned}x' &= u / w \\y' &= v / w\end{aligned}\quad (12)$$

where

$$[u \quad v \quad w] = [x \ y \ 1]T \quad (13)$$

and T is the 3x3 matrix:

$$T = \begin{bmatrix} a & d & g \\ b & e & h \\ c & f & 1 \end{bmatrix} \quad (14)$$

Compared with the affine transform, the extra point (or 2 parameters) allows specification of perspective effect by the relative distances between pairs of points. Because the projective transform is not linear, it cannot be composed as a sequence of translations, shears, scaling and (optionally) rotations.

The eight coefficients in (11) can be calculated from four corresponding pairs of control points on two surfaces. No three points may be collinear.

Control Points and Fiducial Design

As the description above, the proposed projective transformation function relies on control points to calculate the transformation parameters. In the case of dermatology, the pathological progression is to be assessed and invariant features are necessary to compensate perspective variation. Based on the deformation of skin, and pathological characteristics of the skin lesion, there is a lack of skin-based features that are invariant enough to solve the transformation function.

To solve this problem, a rigid fiducial marker design is proposed with invariant control points to meet the demand of invariant geometric features.

Design

To provide higher level reliability, six corresponding pairs of points will be inferred from the centroids of six square fiducial marks. No three points are collinear. The white surface of the marker is used for color correction and will be discussed in detail in following sections. The figure 5 below is the fiducial marker design:

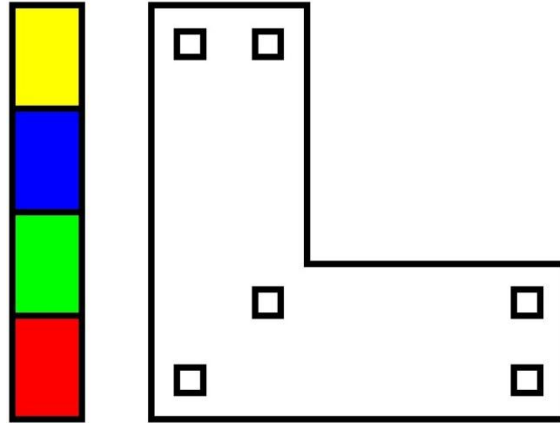


Figure5 Fiducial marker

For potential automatic process in the application, square fiducial is used. In Figure 5 and 6, each square fiducial provides four ideal corner points for the sensor to capture. The straight edges of a square can be used to compute best-fit lines allowing corners to be computed with greater and potentially sub-pixel accuracy. The 1.5cm x 1.5cm fiducial marker is sticky back and is designed to be applied on the skin close to lesion tissue. The stickiness ensures the marker stay invariant for a short period of time when the image is taken or telemedicine is under way.

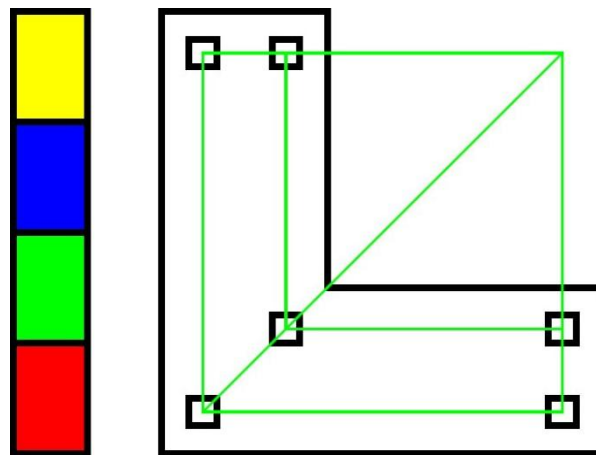


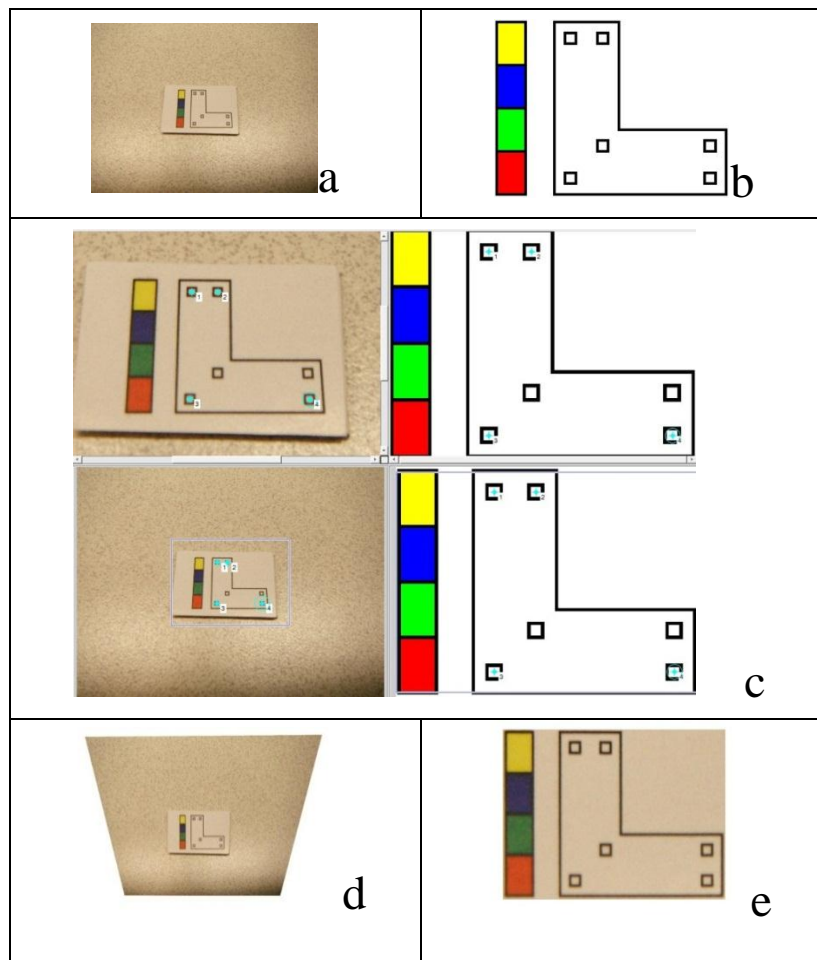
Figure6 Fiducial alignment

The green reference lines show desired alignment of centroids and diagonals after a geometric registration

Skin Lesion Imaging and Image Registration Process

- Apply the marker on the skin near the tissue lesion
- Take the fiducial marker and the skin lesion into one image
- Register the image with a reference image of a desired perspective
- Overlay the regions of interest in two images for pathological study

Below is an example in Figure 7 of registering a fiducial marker which is taken from a certain camera perspective. The image with perpendicular perspective of the prototype fiducial marker of high resolution is used as reference and is called reference image (Figure 7b). An image taken from non-perpendicular perspective is called target image (Figure 7a) and is to be aligned to the reference image.



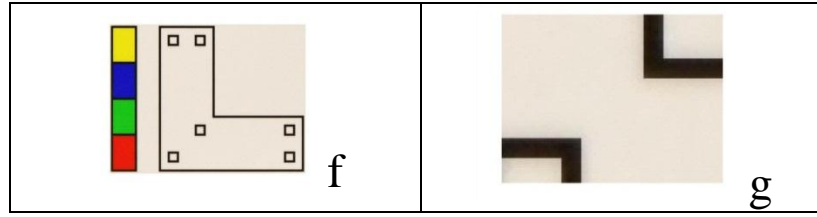


Figure 7 Perspective alignment by control points

First row: a, the raw image data; b, the reference fiducial marker with perpendicular perspective

Second row: c, the process of choosing four pairs of control points

Third row: d, the resulted image after perspective correction; e, the cropped image with region of interest

Fourth row: f, overlap the resulted and the reference images; g, the residual error

Experiment of Perspective Alignment

The perspective alignment in following experiments is through the proposed projective transformation function and reverse mapping of the input image (target image) which transform the input space into the same perspective of the reference image. Experiments use a standard scene to test the performance of the proposed method and fiducial marker design. After the perspective alignment, both target and reference images are aligned in the same space with same size. Both are converted into binary format, and then an absolute difference between the two binary image matrices is calculated. The pixel count of absolute difference and its percentage of all image pixels of the black printed area are calculated and used as residual error measure.

The detailed process and programming can be found in Appendix F.

Experiment I

Objective: show that the proposed method of perspective alignment and fiducial marker can be used to restore a standard view of the scene when the camera is at different distance but similar angles (perspectives). Result is listed in Figure 10.

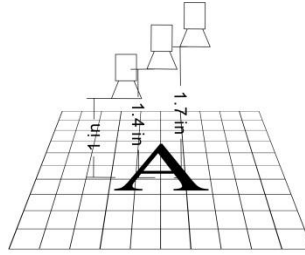


Figure 8 Illustration of camera geometry in Experiment I

From the perspective alignment result below in Figure 9, the absolute difference between the print and the standard computer graph shows visible residual error after the registration process. The print spray on the paper is the major cause for the error. Hence, for later experiments, one printed and registered image with perpendicular perspective is chosen as reference image for little difference in the ground truth.

The experimental result is shown in Figure 10. The absolute difference between two images is less than 0.5% in pixel counts.

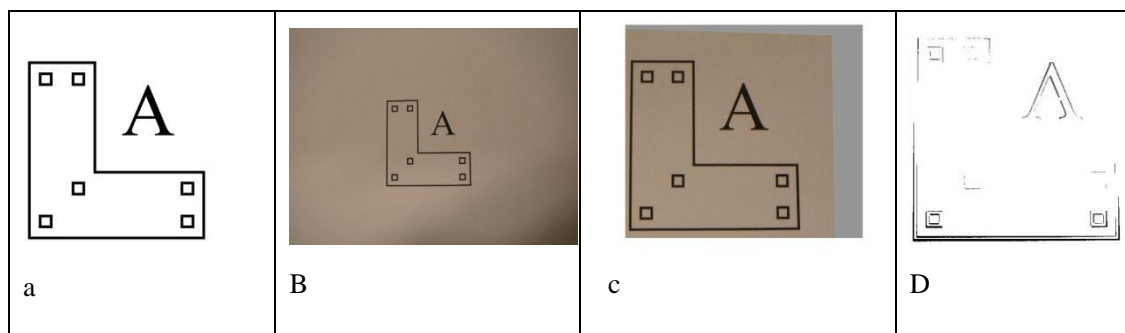


Figure 9 Perspective alignment of a computer graph and print of a standard scene

Figure a is a computer graph of standard reference with perpendicular perspective

Figure b is the printed version of figure a

Figure c is the result of figure b after registration to the perpendicular perspective of figure a;

Figure d is the binary format of the residual error which is mainly caused by print spray on the paper and error in manual choosing control points

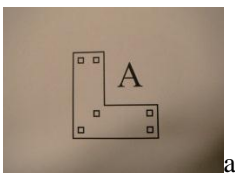
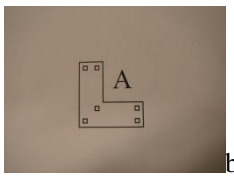
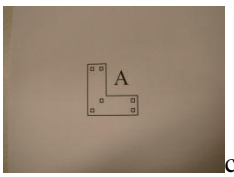
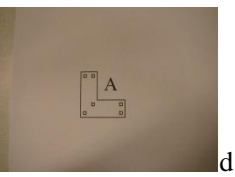
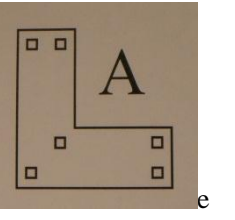
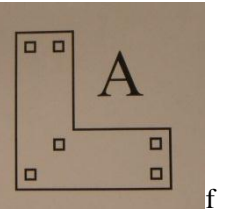
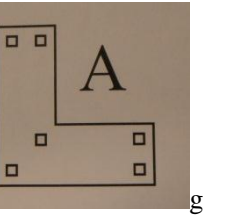
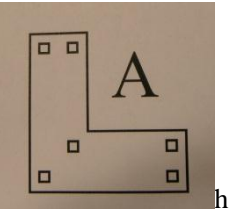

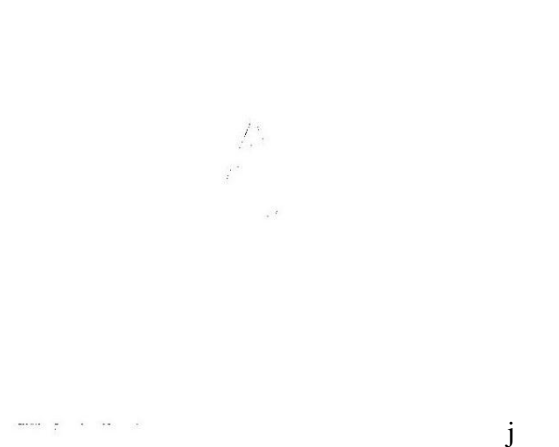
| | | | |
|--|---|---|---|
|  a |  b |  c |  d |
|  e |  f |  g |  h |
| The absolute difference: 100 pixel Percentage of difference ≈ 0 | The absolute difference: 140 pixel Percentage of difference ≈ 0 | The absolute difference: 1350 pixel Percentage of difference ≈ 0.41 | The absolute difference: 720 pixel Percentage of difference ≈ 0.23 |
|  i | |  j | |

Figure 10 Result of Experiment I

First row: a b c d: images taken with similar camera perspective but different distance (approximately 50cm, 40cm, 30cm, 20cm)

Second row: e f g h: the resulted images after perspective alignment

Third row: percentage of difference after perspective alignment

Fourth row: i j: the visible residual error for figure c and d after perspective alignment

Experiment II

Objective: show that the proposed method of perspective alignment and fiducial marker can be used to restore a standard view of the scene when the camera is at

different angles (perspectives) but similar distance. Result is listed in Figure 12.

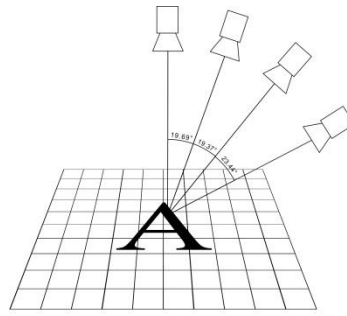


Figure 11 Illustration of camera geometry in Experiment II

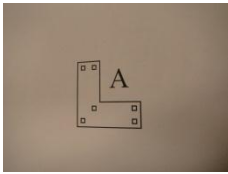
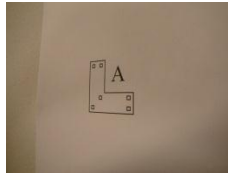
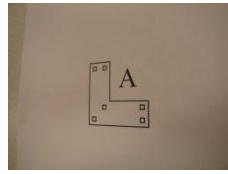
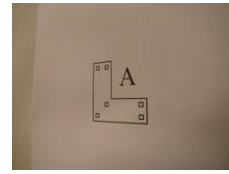
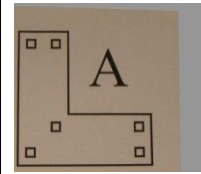
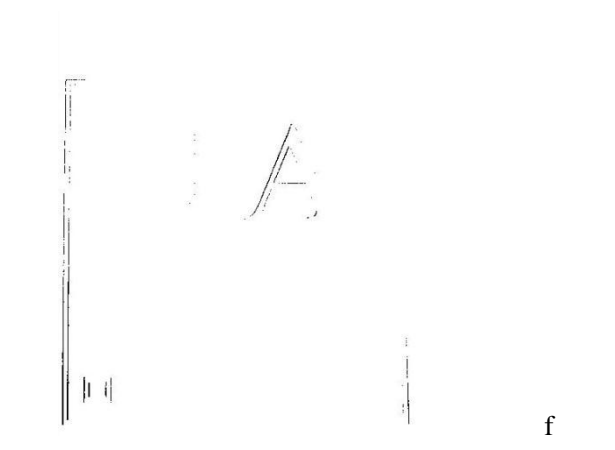
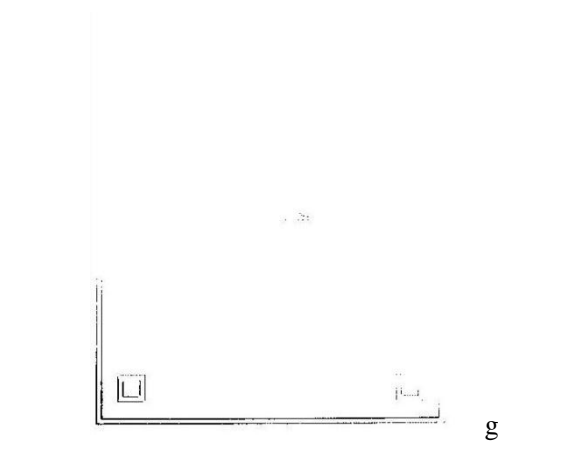
| | | | | |
|---|--|--|--|--|
|  |  |  |  |  |
| a | b | c | d | e |
| The absolute difference: 120 pixel Percentage of difference ≈ 0 | The absolute difference: 200 pixel Percentage of difference ≈ 0 | The absolute difference: 1350 pixel Percentage of difference ≈ 0.41 | The absolute difference: 2018 pixel Percentage of difference ≈ 0.62 | |
|  | |  | | |
| f | | g | | |

Figure 12 Result of Experiment II

First row: a b c d: images taken with different camera perspective (with angle of 80, 50, 40 and 35) but similar distance; e: the reference image

Second row: percentage of difference after perspective alignment

Third row: the visible residual error for figure c and d after perspective alignment

Experiment III

Objective: show that the proposed method of perspective alignment and fiducial marker can be used to restore a standard view of the scene when the scene is imaged from random perspective, distance, and rotation factor. Result is listed in Figure 13.

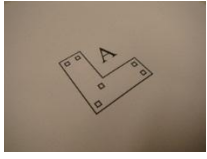
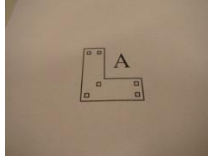
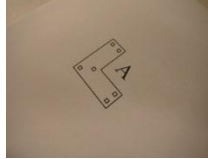
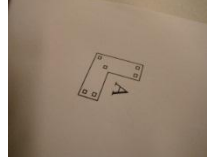
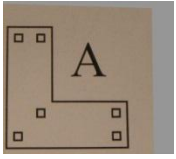
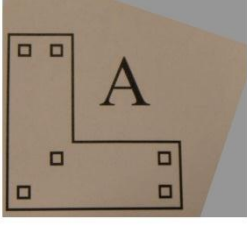
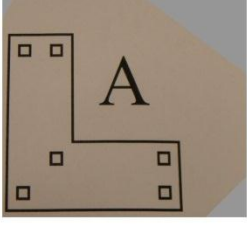
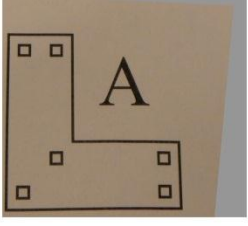
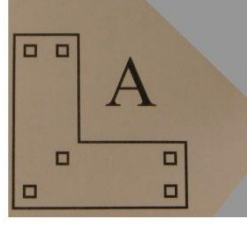
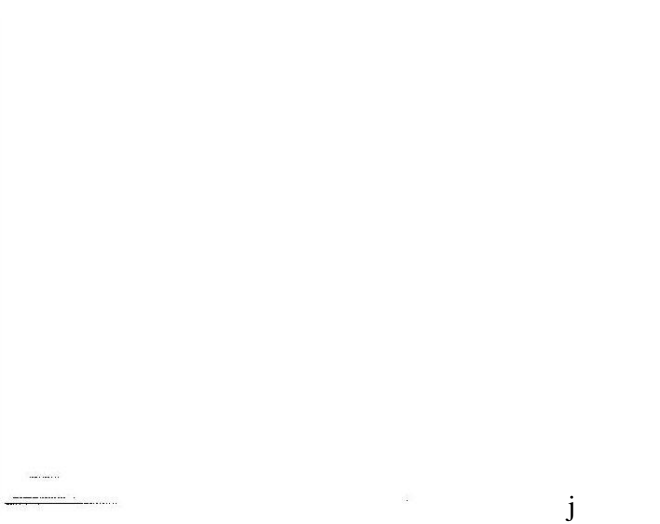
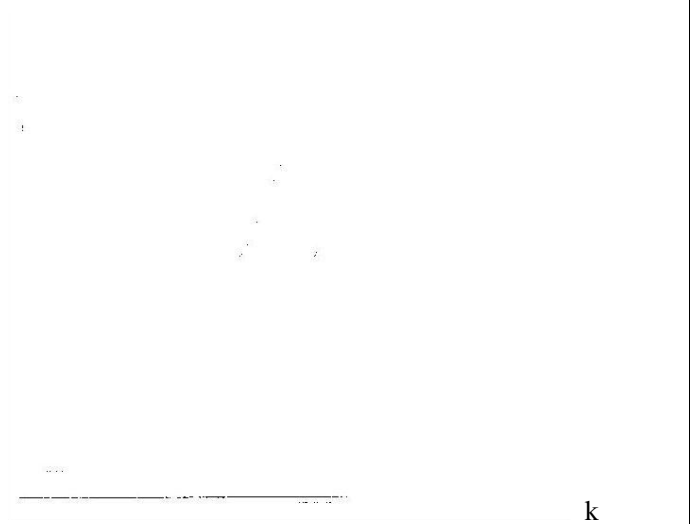
| | | | | |
|---|---|--|---|---|
|  |  |  |  |  |
| A | B | c | d | e |
|  |  |  |  | |
| f | g | h | i | |
| The absolute difference: 171 pixel Percentage of difference ≈ 0 | The absolute difference: 200 pixel Percentage of difference ≈ 0 | The absolute difference: 1208 pixel Percentage of difference ≈ 0.37 | The absolute difference: 342 pixel Percentage of difference ≈ 0.11 | |
|  | |  | | |
| j | | k | | |

Figure 13 Result of Experiment III

First row: a b c d: taken with random perspective, distance and rotation factor; e: reference image

Second row: f g h i: the resulted images after perspective alignment

Third row: percentage of difference after perspective alignment

Fourth row: j k: the visible residual error for figure c and d after perspective alignment

Shifted Fiducial Marker Location

In the case of follow-up study of tissue progression, the imaging is done periodically. Hence, every time the image is taken, the fiducial marker is placed with geometric variation compared with last-time location. Given this case of variable fiducial marker location, the projective transformation does not align skin lesion features directly. After the perspective alignment, the geometric variation still exist which is mainly on two-dimensional shift and rotation factors. Such an effect is shown in Figure 14 below.

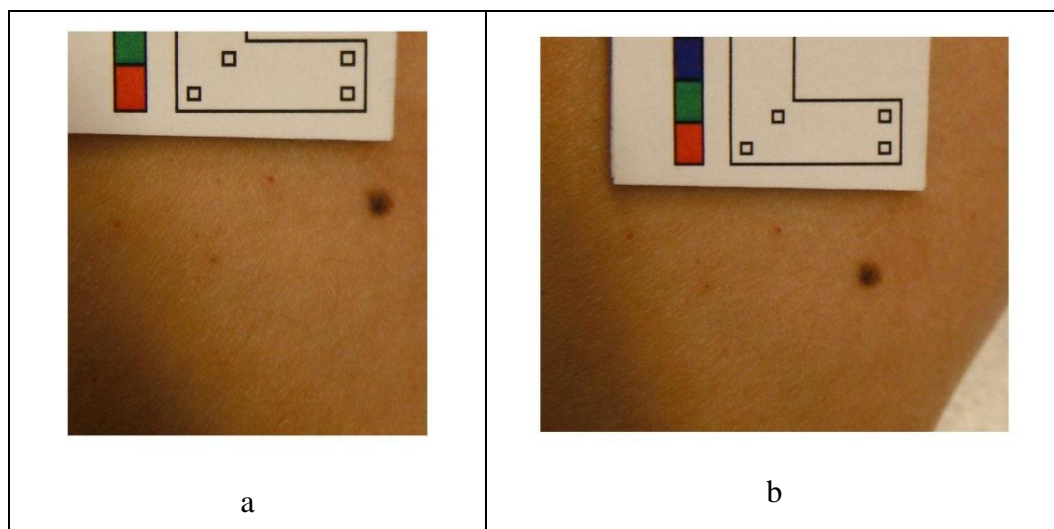


Figure 14 Variable location of fiducial marker

Image a and image b of the same skin lesion share the same perspective after perspective alignment while due to the shifted fiducial marker location, the two skin lesion areas are not matched due to rotation factor.

B. McGregor [8] proposed an algorithm for geometrically registering pairs of images of multiple skin lesions. Multiple lesion features are used as new control points and the remaining geometric distortion can be restored by a second geometric transformation.

The principle is similar to the fiducial-point based method demonstrated above. However, McGregor's method is based on the assumption that the skin surface has restorable or little deformation between two imaging processes. Under which case, all spots on the skin can be used as new control points to infer the parameters of the

second transformation function [8]. This method is tested and result is figured below.

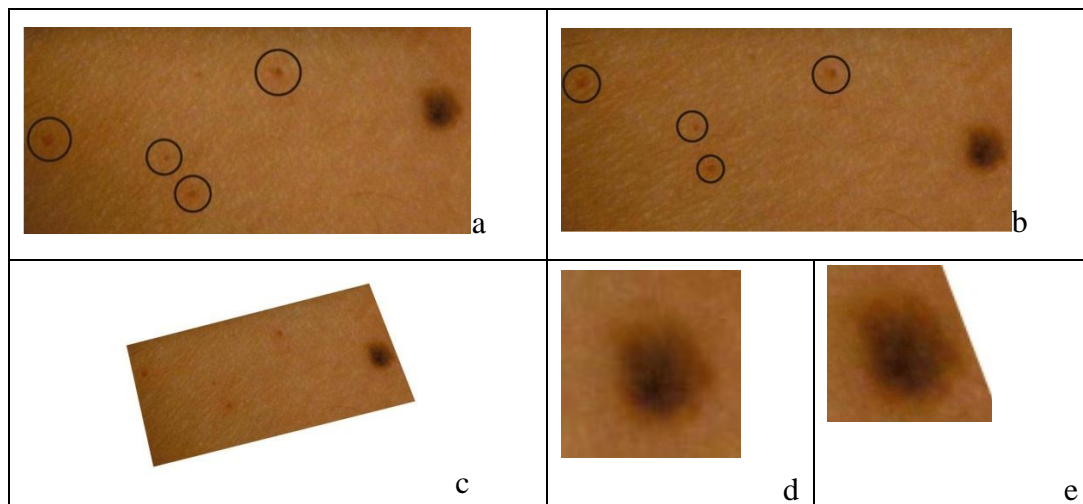


Figure 15 Further registration using McGregor's Method

First row: a: reference image; b: target image; control points are circled in both images.

Second row: c, the registration result of the target image

Second row: d is cropped skin lesion from the reference image; e is the cropped skin lesion from the registered image

Discussion

The above registration process of a standard view of the scene with the reference image gives residual error from 0 to 0.62%. The pixel defects shown of absolute different between two images are mainly caused by error in manual locating control points.

From above experimental result, it is concluded that a projective transformation can well correct perspective distortion and align features with accuracy. This conclusion is based on met assumptions of zero deformation of fiducial marker in use, accurate control points locating and relatively planar skin surface. Give the geometric residual error ranging from 0 to 0.62% in experiment result, a 1% growth of lesion tissue can be used as lower limit of detection of the proposed method.

However, with better fabrication, fiducial marker can be made of rigid material to

avoid deformation. The fiducial feature can be precise and small enough that locating by the skin lesion with negligible third dimensional features; more accurate control point's location can be achieved by automatic detection of square features.

In a more practical use condition, below factors may cause variability in perspective alignment result:

- Attach the fiducial marker outside the effective range
- Camera geometry that causes loss of lesion information
- Misalignment of control points in a manual process

Given the scope of this thesis and limitation on fabrication, above expectation and sources of variability can be topics for future work. However, the efficacy of the proposed parametric and fiducial method is proven in aligning two-dimensional skin lesion images.

3.2 Color Correction

Proposed Method

Illumination estimation in photography and image processing is widely based on standard color reference and the responsive estimation of illuminant color effect on the reference [10] [11] [12] [13] [24]. In related applications, color reference such as white card, gray card, color charts are widely accepted for color constancy due to their real-time color information and relatively stable color change under certain illuminant types [22] [23] [25].

Context of Skin Lesion Imaging

Periodic screening of skin lesion is a major approach for early detection of skin cancer which enables early diagnosis, treatment and reducing death rate. With the rise of telemedicine in recent years, many medical assessments can now be conducted online, either through video or still image. In the case of skin lesion screening, the first step is usually visual assessment. The lesion color and the color change over time are two essential features for diagnosis. Quantification of lesion color feature is of

essential diagnostic importance [1] [2] [3] [7].

In both real-time and follow-up assessment, unavoidable scene shift caused by human body movement often leads to different angle towards the illumination. A variation of illumination at different times of imaging also exists.

Practical Limitation

- The users of the camera can be patients, medical practitioners, and anyone else other than professional photographers.
- The cameras used can be of a wide variety: those professional ones with the capability to shoot and store in RAW file; and those commodity-like cameras that usually store only in JPG file.
- Different CCDs from different manufacturers present different responses to the same scene.
- For some of those commodity-like cameras, a certain level of in-camera white balance and exposure setting are often automatic and cannot be shut off.
- Raw file is often used in professional photography. However given the size of the file, it is not suitable in this case. Furthermore, different manufacturers store RAW file in different ways and cause a lack of generality.
- The detailed CCD performance is generally proprietary because of commercial interest. The total camera response, namely, the CCD response + in-camera software processing, is also unavailable.
- In the real-time case, the sensed color variation in the scene can be caused by illumination, exposure, and reflectance angle. Over a period of time, local pathological progressions of the lesion and skin tone change are very possible.

Recall the Color Constancy Problem

Given above assumption, it is necessary to recall the color constancy problem in previous section.

The image values f (the ideal camera response) for a Lambertian surface depend

on the illuminant spectra $e(\lambda)$, the surface reflectance $s(x, \lambda)$ and camera response function $c(\lambda)$, where λ is the wavelength of the light and x is the spatial coordinate:

$$f(x) = \int e(\lambda) s(x, \lambda) c(\lambda) d\lambda, \quad (7)$$

assuming that the scene is illuminated by one illuminant and that the observed color of the illuminant spectra e depends on the spectra of the illuminant source $e(\lambda)$ and the camera response function $c(\lambda)$ then the solution to the estimation of e is:

$$e = \int e(\lambda) c(\lambda) d\lambda \quad (8)$$

- In practical use, the illumination source might be multiple and are often unknown.
- The sensed surface reflectance from the scene, namely the CCD response is unknown; given the compulsory in-camera processing of the sensed image and further given various CCDs and processing principles the estimation of $c(\lambda)$ is impossible.

in short, the only item from the above function that the user would have is the sensed image. Given the sensed image values s , both $e(\lambda)$ and $c(\lambda)$ are unknown, the problem of estimating illuminant color is under-constrained, and the goal of color constancy is unattainable without further assumptions.

White-Patch Method Based on White Reference

In order to estimate the illumination, a fiducial marker with White Reference patch is designed for color correction. The average R, G, and B values from the white reference is calculated and used as the brightest point R_w, G_w, B_w values in the image data.

The gain value for three color channels = $(255/R_w, 255/G_w, 255/B_w)$

$$R_g[i, j] = R[i, j] \times 255/R_w$$

$$G_g[i, j] = G[i, j] \times 255/G_w$$

$$B_g[i, j] = B[i, j] \times 255/B_w$$

where (R, G, B) is the original color, and (R_g, G_g, B_g) is the corrected color.

The detailed steps and programming can be found in Appendix B.

Color Reference Design

The proposed color reference is incorporated with the fiducial marker for image registration. The white surface on the fiducial marker is used as white reference for illuminant effect estimation and subsequent color correction. A four-color stripe is added on the left side of fiducial marker for visual evaluation of the correction results.

In Figure 16, image a is the computer graph of the fiducial marker design.

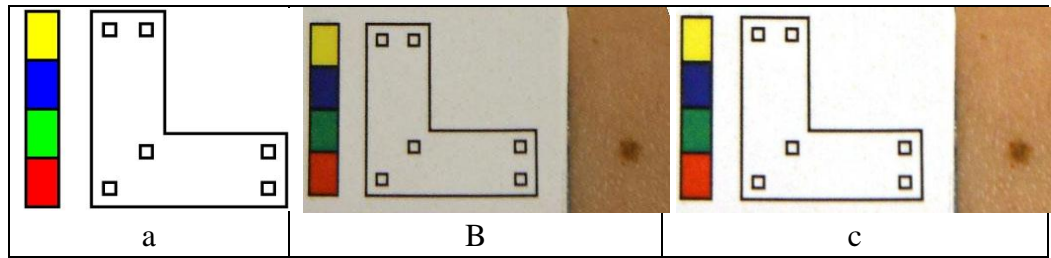


Figure 16 Color correction demonstration

Image a: the computer graph of the color reference design

Image b: sensed image after perspective alignment with a perpendicular perspective

Image c: the resulted image after color correction using proposed method

Fabrication

High quality A4 print paper is used as surface material. Printing is done by an EPSON NX410 color printer. The surface is glued onto a thin piece of plastic board to avoid deformation.

Experimental Setting for Image Acquisition

A commodity-like FUJIFILM XP20 digital still camera is used to capture all the

images in the test dataset. All images were recorded as sRGB color representation in JPEG format. The camera outputs 8-bit data per channel so the range of possible digital counts is 0-255. The sensed image contains 4320 x 3240 8-bit values in sRGB pattern. To create an image, on average 3 megabytes are used.

Shooting mode is fixed at “Program Auto” for the camera under which most automatic processing is shut off except for shutter speed and/or aperture setting. The exposure value which denotes all combinations of the camera’s shutter speed and relative aperture is decided by the camera automatically to give same or similar exposure. The CCD sensitivity is fixed at ISO 200. This relatively fixed setting is for this camera to make least possible color artifacts and the output is nearest to the pure CCD response. Given automatic configuration on shutter speed and/or aperture setting, the camera-caused deviation across different illuminations exists while its effect on the resulted images is throughout the whole image. The camera’s built-in automatic white balance is compulsory. Given the unknown automatic white balancing principle of this camera, the color balancing effect on the sensed images is of interest and will be studied in the experiment.

To study the color correction performance of the proposed method, four experiments with four different illuminations are designed and listed in the next section with their respective setting. Three concerned factors are camera geometry, fiducial location and illumination type and intensity. A number of images are taken under the same illumination for each experiment. Camera geometry and fiducial location are slightly changed corresponding to the condition of follow-up study on skin lesion progression over time. Given the assumption of uniform illumination over the scene, a shifted fiducial location should not present significant effect on color correction result. Between taking two images, the camera is refocused and its perspective towards the scene is moved slightly. Under the hypothesis of planar surface of the skin lesion, surrounding skin and the neighboring surface of the color reference (with fiducial marker), the same depth in the scene is assumed. For a uniform focus result across all images, the focus is adjusted according to the planar surface of the color reference in the scene each time.

The color reference (with fiducial marker) is placed in the scene where close to the skin lesion of interest and the local illumination incident is assumed to be same or similar to the scene illumination. Theoretically, the variation between the illuminations on the color reference and the target skin lesion exist because of inter-reflection, conditions resulting in obvious variations in illumination across the scene are avoided. For example, parts of the scene are shadowed by physical object; areas in the scene are illuminated by different illuminants.

To reduce redundancy caused by irrelevant surrounding skin area, the image is cropped such that an image window covering skin lesion and the color reference are kept in the resulted image.

Given the proposed method, the effect of the illumination is estimated by manual cropping the sensed images for white patches from the color reference and sampling and averaging RGB digital counts from the segmented white patches.

Given previous research in photography and medical imaging implementation, the light of the illuminant should be delivered onto the surface at an angle of 45° and the reflectance from the object surface should be sensed by the camera CCD at 0° to the surface normal. This is an internationally established imaging geometry for color measurements for least possible shadows and reflections [1] [16]. Given the practical conditions of use, a uniform illumination a precise 45° of incident light angel is difficult to engineer. However, a direct lighting onto the sensor should be avoided in case of erroneous in-camera white balance. Throughout the image acquisition process for the experiments, the camera is not faced towards light source and an incident light angel greater than 45° is most commonly used [1] [16].

Because the human skin is irregular surface, a lateral camera perspective towards the skin lesion of interest often causes loss of diagnostic features. Hence, for camera geometry, a lateral perspective is avoided.

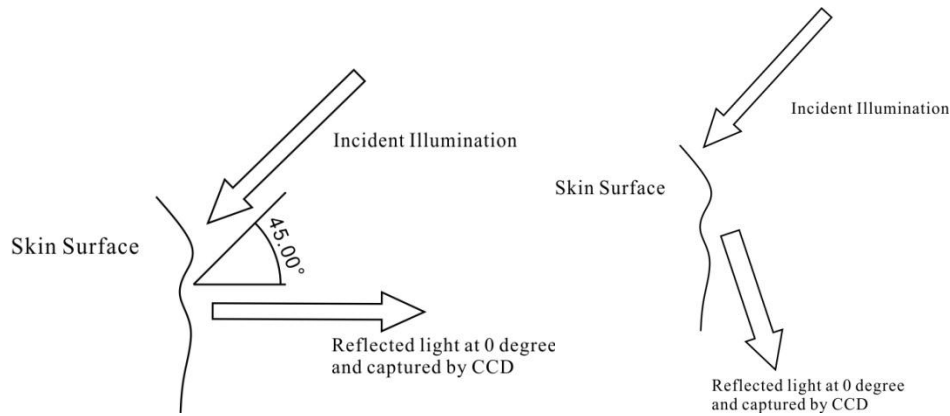


Figure 17 Imaging geometry

Left: the standard illumination and camera geometry for color measurement

Right: a lateral camera geometry leading to loss of diagnostic features

Experimental Design and Imaging Conditions

Given the practical conditions of use, the factors that may affect the color performance include:

- Illumination type and intensity
- Illumination geometry: angel of incident illumination on the skin
- Camera geometry: camera perspective, camera angel to the illumination.

The illumination is major source of color variation. Hence color correction process is tested under four types of illumination. The illumination and camera geometry as discussed in previous section will be handled with the least amount of engineering whose purpose is to preserve the lesion features in the image. Given above factors, four experiments are designed and respective sets of images are taken. After the color correction, its effect will be described by numerical measures for within-group color variation and between-groups color variation. Four types of illumination are used: multiple fluorescents lights, single fluorescent light, day light and tungsten bulb (incandescent light).

Experiment IV

- Multiple fluorescent lights with uniform illumination on the skin and fiducial
- Shifted fiducial location on the skin throughout the imaging process

- Variable camera perspectives

Experiment V

- Single fluorescent light with uniform illumination on the skin and fiducial
- Shifted fiducial location on the skin throughout the imaging process
- Variable camera perspectives

Experiment VI

- Daylight with uniform illumination on the skin and fiducial
- Shifted fiducial location on the skin throughout the imaging process
- Variable camera perspectives

Experiment VII

- Tungsten Light with uniform illumination on the skin and fiducial
- Shifted fiducial location on the skin throughout the imaging process
- Variable camera perspective

Performance Metrics

The performance of color correction can be subjectively evaluated by numerical metrics expressing the properties of the resulted skin lesion images.

Given the experimental design, only one skin lesion is photographed for each set of images within a short period of time. The pathological progression and skin surface deformation are considered negligible. Hence, after the correction, the residual variation of color features is considered error which is to be quantified for accuracy assessment.

Image Segmentation

For the accurate quantification of the geometric and color features, image segmentation is necessary to enable the focus on skin lesion digital counts and simplify the extraction of numerical information [1] [2] [3].

Given the purpose of using image segmentation in this research, a widely

accepted segmentation procedure that uses image filter, intensity value threshold and binary mapping is chosen. There have been many other segmentation methods and procedures proposed in recent years; however an in-depth research and comparison of them are not the focus of this thesis.

The principle of the chosen method relies on the fact that the intensity values of lesion pixels differ from the surrounding normal skin surface. By choosing upper and lower value boundaries, the lesion color-like pixels are possible to be isolated. With an estimated contour, the skin lesion area can be segmented. The numerical metric then can be calculated on the pixels counts that locate in the contour other than the whole sensed image [1] [14]. One example is listed in Figure 18. The original image a is first filtered with upper and lower value boundaries to reduce noise. Then a binary (black and white) mapping is generated by intensity value threshold. Finally, the skin lesion area is cropped.

The detailed steps and programming can be found in Appendix C.

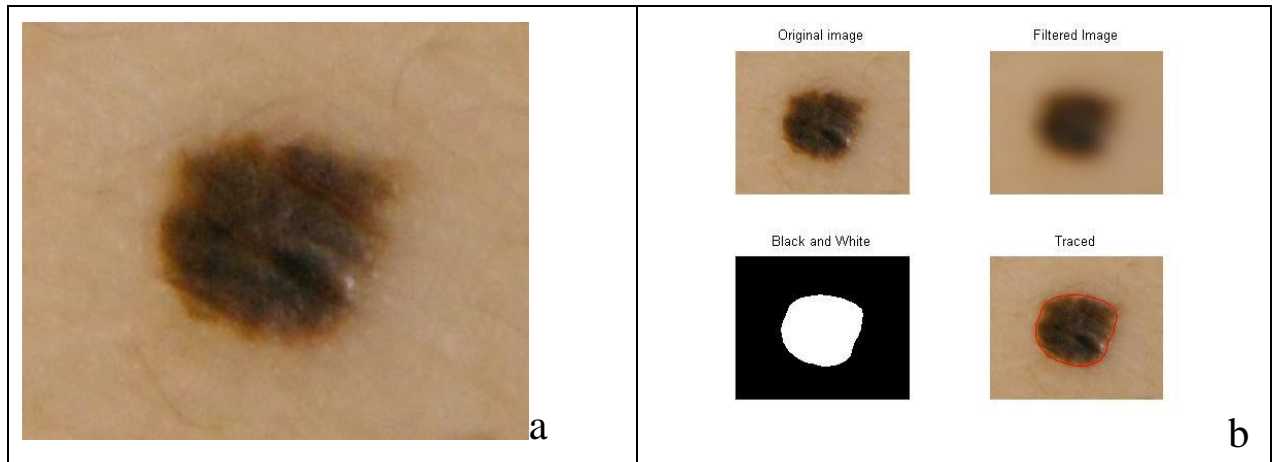


Figure 18 Skin lesion image segmentation

a: the original image

b: the original image; filtered image; black white binary mapping; traced boundary of skin lesion area

Geometric Metrics

The overlapping method is introduced in previous chapter of methodology. Given the negligible amount of variation after the perspective alignment, no further quantification is necessary. Furthermore, the residual variation is mostly caused by

skin and/or muscle tissue movement which are considered normal in real use. The fine fabrication and small size of fiducial marker that better fits the skin surface can reduce the residual variation which can be a part of future work.

Color Metrics

For an objective evaluation of color correction performance, a numerical metric is necessary to express the color properties of the sensed image.

The skin lesion in each sensed image is segmented and then the average values and pixel-wise standard deviations of R, G and B channel values are calculated for each corrected image. Sets of skin lesion images taken under different experimental settings are used. Results are compared within each set and across multiple sets.

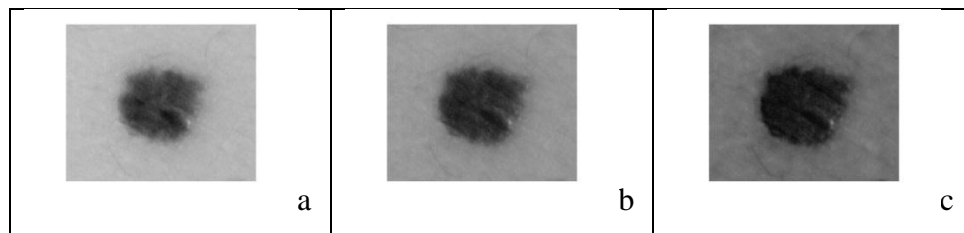
The detailed procedures and programming can be found in Appendix D.

Another widely accepted color difference measurement based on CIEL*a*b* color space is also used to describe the residual error after the color correction. The CIEL*a*b* color space and related color difference formula were first proposed by Commission Internationale de l' Eclairage and used in color measurement [22].

The mean values of L*, a*, and b* channels of a group images are calculated and used as standard value; the mean values of L*, a*, and b* channels of each image are used as sample values.

The ΔL^* , Δa^* , and Δb^* values are calculated from the subtraction of sample values from standard values. Color difference is calculated using the formula below:

$$\Delta E_{ab}^* = \sqrt{(\Delta L^{*2} + \Delta a^{*2} + \Delta b^{*2})} \quad (15)$$



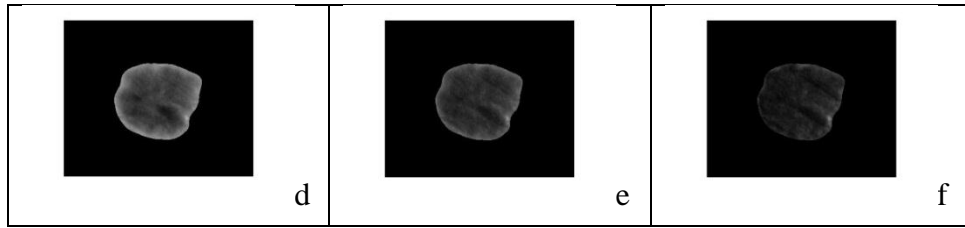


Figure 19 R, G and B channel intensity values

First row: a, b, c: intensity values of R, G and B channels expressed in gray level

Second row: d, e, f: the segmentation of the lesion area and the intensity display

Result of Color Correction

Based on the experimental setting, 15 images are taken of the same skin lesion for each experimental set. The image segmentation is applied first on the skin lesion area. The test result shows that with the same type of illumination, for example, between Experiment IV and V, the mean difference is only 1.5-3 for average RGB values after correction. The daylight and tungsten illumination result in respectively bluish and yellowish image after correction. After color correction, the color difference between groups of images taken under different illumination types exists. For inter-illumination case, the tungsten lamp and daylight corresponds to highest difference value from 20-30 in the 0-255 scale and the residual color distortion is visible.

After the analysis of numerical color metrics, and comparing them with the original camera response and digital imaging information, it is found that in Figure 20 the first and fourth images were taken with a higher brightness value which was a product of an automatic white balance. The automatic in-camera processing can be triggered by a light sensor and the white balance parameters were estimated by in-camera program automatically. The automatic white balance obviously is non-linear, namely the white patch and skin lesion are processed differently. After the color correction the skin area pixel counts have a generally lower value on R, G and B channels while the white patch area is adjusted to the RGB value (255, 255, 255) under hypothetical canonical illumination.

The same case happens to all other images that have a large deviation from the

mean with-in group RGB value. The trace of automatic white balance is also found and the brightness values are exceptionally high. This problem can be solved by turning off all automatic functions in digital camera. Unfortunately some cameras make the function compulsory. Given the nonlinear white balance processing, the gourd truth is difficult or impossible to be restored without the knowledge of the proprietary algorithms from the manufacturers. The possible solution for the same set of images is the excluding of those white-balanced images since their color distortion cannot be accurately compensated for. Result is presented in Table 1, 2, 3 and 4.

Experiment IV

- Multiple fluorescent lights with uniform illumination on the skin and fiducial
- Shifted fiducial location on the skin within 10cm's range of the lesion centroid
- Variable camera perspectives

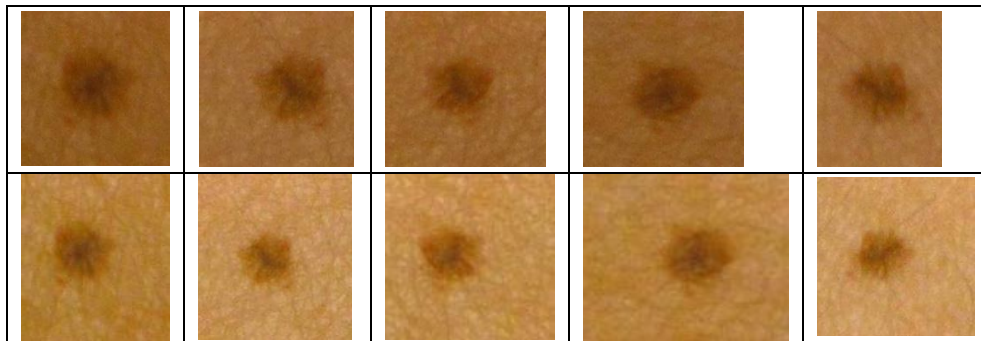


Figure 20: Color correction result of Experiment IV

The first rows of images are original and taken under multiple fluorescent lamps; the second row shows the results after color correction.

Table 1

Experiment Result IV

| One fluorescent light | Before Correction | After Correction |
|-----------------------------------|---------------------------|---------------------------|
| | Absolute (in 0-255 scale) | Absolute (in 0-255 scale) |
| Maximum Difference for Mean Value | 23.4 | 15 |
| Maximum Difference | 14.7 | 8.3 |

| | | |
|--------------------------------------|----------|----------|
| for Pixel Intensity Variegation | | |
| ΔE_{ab}^* values range | 0.83-4.3 | 0.4-3.6 |
| 95% C.I. of ΔE_{ab}^* values | 0.56-5.8 | 0.29-4.1 |

Experiment V

- Single fluorescent light with uniform illumination on the skin and fiducial
- Shifted fiducial location on the skin within 10cm's range of the lesion centroid
- Variable camera perspectives

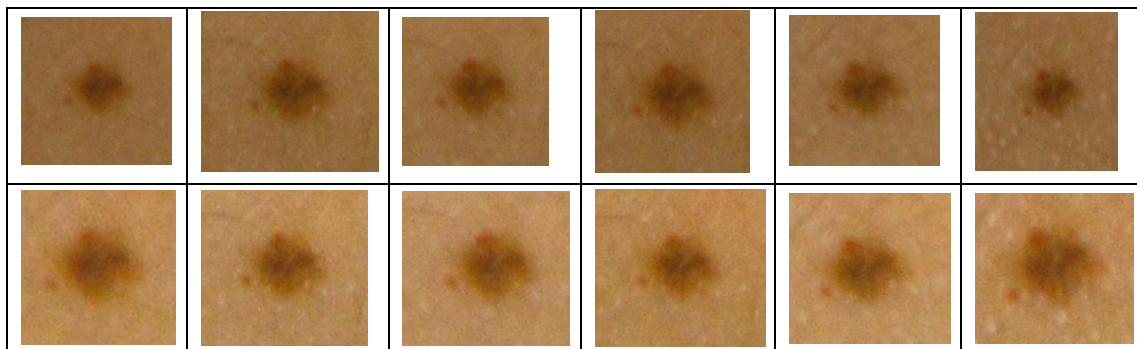


Figure 21: Color correction result of Experiment V

The original images were taken under single and constant fluorescent light.

Table 2
Experiment Result V

| One fluorescent light | Before Correction | After Correction |
|-----------------------------------|---------------------------|---------------------------|
| | Absolute (in 0-255 scale) | Absolute (in 0-255 scale) |
| Maximum Difference for Mean Value | 11.2 | 5 |

| | | |
|--|----------|----------|
| Maximum Difference for Pixel Intensity Variegation | 8.6 | 4.3 |
| ΔE_{ab}^* values range | 0.64-4 | 0.43-2.5 |
| 95% C.I. of ΔE_{ab}^* values | 0.44-3.6 | 0.31-2.8 |

Experiment VI

- Daylight with uniform illumination on the skin and fiducial
- Shifted fiducial location on the skin within 10cm's range of the lesion centroid
- Variable camera perspectives

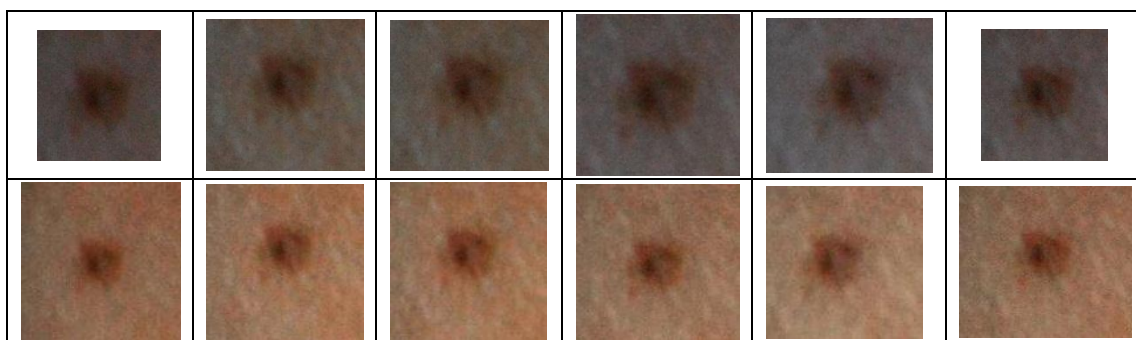


Figure 22: Color correction result of Experiment VI
The original images were taken under the daylight.

Table 3
Experiment Result VI

| Daylight | Before Correction | After Correction |
|-----------------------------------|---------------------------|---------------------------|
| | Absolute (in 0-255 scale) | Absolute (in 0-255 scale) |
| Maximum Difference for Mean Value | 3.8 | 2.7 |

| | | |
|--|----------|----------|
| Maximum Difference for Pixel Intensity Variegation | 2.1 | 1.8 |
| ΔE_{ab}^* values range | 0.9-3 | 0.6-2.7 |
| 95% C.I. of ΔE_{ab}^* values | 0.67-4.1 | 0.38-2.9 |

Experiment VII

- Tungsten Light with uniform illumination on the skin and fiducial
- Shifted fiducial location on the skin within 10cm's range of the lesion centroid
- Variable camera perspective

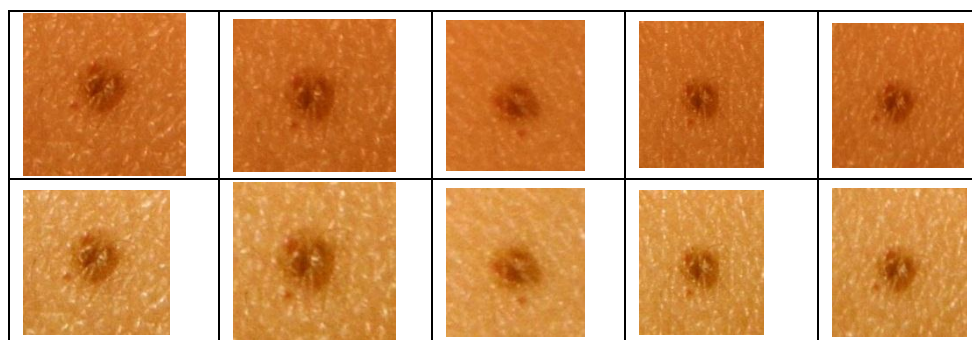


Figure 23: Color correction result of Experiment VII
The original images were taken under the same tungsten light.

Table 4
Experiment Result VII

| Single tungsten light | Before Correction | After Correction |
|-----------------------------------|---------------------------|---------------------------|
| | Absolute (in 0-255 scale) | Absolute (in 0-255 scale) |
| Maximum Difference for Mean Value | 9.4 | 4 |

| | | |
|--|---------|----------|
| Maximum Difference for Pixel Intensity Variegation | 3.4 | 2 |
| ΔE_{ab}^* values range | 1.2-4.4 | 0.35-2.8 |
| 95% C.I. of ΔE_{ab}^* values | 0.7-4.8 | 0.3-3.05 |

Table 5
Mean RGB values of multiple image sets

| | R \pm S.D. | G \pm S.D. | B \pm S.D. |
|-----------------------------|------------------|------------------|------------------|
| Multiple fluorescent lights | 159.56 \pm 5.6 | 99.61 \pm 4.47 | 28.96 \pm 5.45 |
| One fluorescent light | 155.58 \pm 0.8 | 99.87 \pm 2.09 | 30.3 \pm 2.31 |
| Daylight | 122.7 \pm 4.8 | 74.56 \pm 3.2 | 49.3 \pm 1.94 |
| Tungsten Light | 182.69 \pm 3 | 102.8 \pm 2.1 | 27.5 \pm 2.04 |

Given the result of above experiments, after color correction, the maximum values of with-in group color variation ranges from 2.7 to 15 (in 0-255 scale) or 1% to 5.9% compared with 3.8 to 23.4 (in 0-255 scale) or 1.5% to 9.2% before color correction. For each within-group color difference, the CIEL*a*b* color difference measurement, a 95% confidence interval of ΔE_{ab}^* values range from 0.29 to 4.1 after correction compared with 0.44 to 5.8 before correction.

During the imaging process, the fiducial location and camera perspective were changed randomly given assumption of imaging geometry. Given 5% significant level of ΔE_{ab}^* value, the within-group color residual error caused by the combined effect of varied fiducial location, and camera perspective is not significant.

To investigate the illumination effect on residual error after color correction, the data is studied group-wise. Given the Experiment Setting IV and V color

performance, the same illumination type but different illumination intensities makes negligible effect after the color correction. The R, G and B value difference between image set IV and V are 1.56%, 0.1% and 0.53%. Given the Setting VI, and VII, the measured between-group difference is significant. Under daylight, the image data after correction has generally lower R and G values and higher B value which make the image bluish. Under tungsten light, the G and B values are within 0.2% variation compared with that under fluorescent light. However, the R value is exceptionally high under tungsten light which makes the resulted image reddish.

From the CIEL*a*b* color difference measurement, the ΔE_{ab}^* value ranges from 0.64 to 3.94 between the two sets of images which were taken under the same illumination type (fluorescent light). A research by Strokes et al., [23] showed that if the CIEL*a*b* color difference is less than 2 or 3 (based on respective conditions), the residual errors after correction will not be visible by naked eyes. Although some residual errors are higher than 3, the color correction process has greatly reduce the color difference both within and between groups of images.

Color Stripe Information

In the fiducial marker, the color strip is used for visual assessment. The RGB value of both cropped color strip and segmented skin lesion are compared and listed below. The data suggest no logical relationship between the skin lesion color and color strip before or after color correction. Hence, the RGB value of color strip is not suitable for a further color correction. An example is listed below in Figure 24 and Table 6. The red patch is cropped and average RGB values are calculated for red patch from each image. For each image, the red patch RGB values are compared with skin lesion RGB values. Based on the numerical measure, the RGB values of color patch and skin lesions have no linear or stable relationship. Given the chosen material and fabrication of fiducial marker, color correction based on color-stripe information tends to present larger within-group and between-group color variation on the skin lesion even when color variation between two color stripes is minimized.

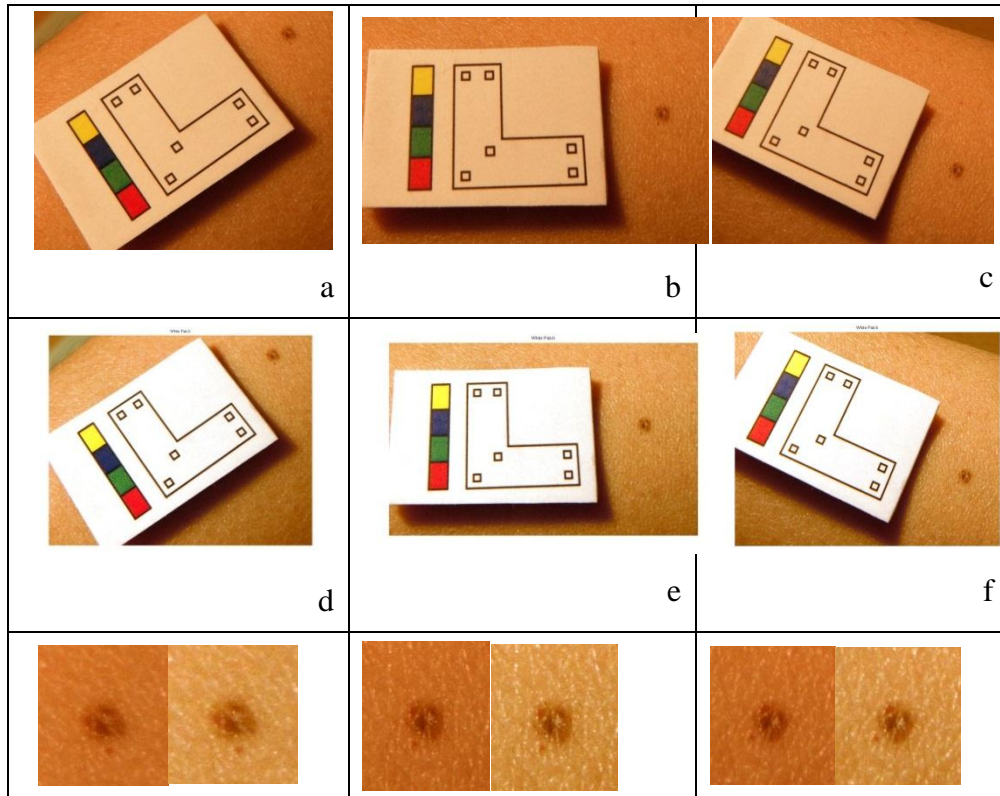


Figure 24 Color correction result

First row: original image a, b, c taken under Experiment Setting VII

Second row: resulted image d, e, f after color correction

Third row: comparing the skin lesion before and after color correction

Table 6

The RGB value of cropped red patch and segmented skin lesion

| Tungsten | Cropped Red Patch | | | Segmented Skin Lesion | | | | |
|----------|-------------------|--------|--------|-----------------------|-------|-------|-------|------|
| | Ravg | 246.33 | 243.15 | 246 | 167 | 166.6 | 176 | |
| Gavg | 53.55 | 34.81 | 23 | 72 | 72.5 | 78 | | |
| Bavg | 37.22 | 32.75 | 32.85 | 14.2 | 13.7 | 15.3 | | |
| Daylight | Cropped Red Patch | | | Segmented Skin Lesion | | | | |
| | Ravg | 228 | 230 | 237.3 | 235.6 | 119.2 | 128.4 | 127 |
| Gavg | 40.7 | 44.5 | 54.7 | 55.46 | 72.7 | 78.6 | 75.5 | 75.6 |
| Bavg | 22.7 | 35.6 | 53 | 52 | 49.3 | 51.1 | 48.3 | 51.2 |

Cause of Residual Error after Color Correction

From resulting data in the previous section, the between-group images which were taken under the same illumination have low color variation (ΔE_{ab}^* values range from 0.64 to 3.94) in segmented skin lesion area. However, the color variation is still significant between the average levels of different image sets taken under respective illumination conditions.

Color variation after correction is mainly caused by two factors: the programmed digital camera response [10] [11] [12] and the fluorescent whitening agent used in printing paper [19].

Commodity-like cameras usually use automatic white-balance, shutter speed, aperture and sensor response which have a certain level of effect on both the within and between-group color residual error. Given the low ΔE_{ab}^* values for within-group comparison, the chosen digital camera gives a stable performance under the same type of illumination. The residual error between different groups is significant which suggest that given different illumination, the camera output and the possible color adjustment are not uniform across the whole sensed scene.

On the other side, the color performance on the white color reference decides the estimation of illumination effect. According to research on white reference materials and respective performance, the fluorescent whitening agent (FWA) and shading dyes [27] used to bleach the paper is one major cause of the variable spectral performance under different type of illuminations [19] [20] [21] which may lead to deviated estimation of illumination effect.

According to large amount of research by N. Pauler, M. Andersson and O. Norberg, many white items used to set the color balance, such as white paper, have fluorescent whitening agents used to make the surface appear white [21] [26] [27]. These whitening agents convert invisible ultraviolet light to visible blue light; counteracting the yellowness of the material and making it look white and bright. The color performance depends on the amount of ultraviolet from the illumination. Illuminants with low ultraviolet light, such as tungsten, will produce a different appearance with an optically brightened paper than fluorescent lighting with a higher ultraviolet component [19] [21].

In short, the FWA absorbs UV light and re-emits it as visible blue color. The effect of the FWA is proportional to the amount of UV-light included in the illuminant. Furthermore, the effect of FWA will be dependent on the actual amount of is used in the paper. Changes in the UV content of the illumination and amount of FWA used in the paper will result in different FWA contributions to the color performance [27].

For example, one most commonly used white colorant is titanium dioxide which does not reflect light evenly across the spectrum. It is yellowish but the human visual system adjusts to make it appear white. A digital camera will sense the slight yellowness and create a slightly blue balance to counteract the yellow. So after the color correction, the images will be slightly bluish.

In Figure 25, and Table 7, given the paper with FWA, from 400nm-420nm, the reflectance of blue is lower than the rest of reflectance spectra. From 420-450nm, the reflectance of blue is higher than the rest of reflectance spectra. Given respective illumination, the paper will give lower blue channel value and higher blue channel value respectively. A color correction based on the white paper surface will consequently give respective bluish and yellowish image on the resulted skin surface.

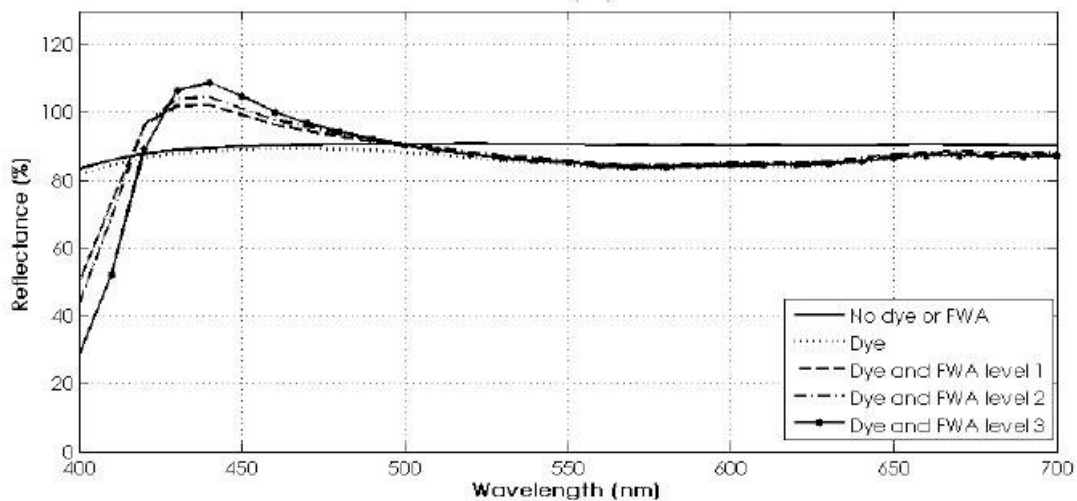


Figure 25: The reflectance spectra of a paper with Fluorescent Whitening Agent given visible spectrum

(From M. Andersson & Ole Norberg. “Color measurements on prints containing fluorescent whitening agents” [21])

Table 7

Spectral colors and respective ranges of wavelength

(From T. J. Bruno, P. D. N. Svoronos. CRC Handbook of Fundamental Spectroscopic Correlation Charts. CRC Press, 2005.)

| Color | violet | blue | cyan | green | yellow | orange | red |
|------------|----------------|----------------|----------------|----------------|----------------|----------------|----------------|
| Wavelength | 380 - 450nm | 450 - 475nm | 476 - 495nm | 495 - 570nm | 570 - 590nm | 590 - 620nm | 620 - 750nm |

M. Andersson [27] suggests that one way to avoid the problem caused by FWA in color calibrations and color measurements on the whole would be to use devices and reference illuminations free of UV light. However, it is admitted this approach relates poorly to the 'real-world' conditions under which printed surface is viewed. Under situations where the image sensor and the color reference use light sources with at least some UV-content, it is possible to correct for the effect of fluorescence given that the UV-content of both light sources is known and that there is a measure of the FWA-content of the printing substrate. More paper samples with known and varying FWA-content must be used in order to obtain a correction model. However, such prerequisites often cannot be met in the context of skin lesion imaging [1], in which case the UV-content is not known and the time and effect in training the correction model is not available.

Recall the color stripes by the left side of the fiducial marker, which is printed with color agents giving respective non-uniform color performance under UV-content. Hence, the color-stripe RGB values are not good estimates for illumination effect given unknown FWA-content, UV-content in the light and automatic camera white balance. From the result of Experiment I, II, III and IV, a color correction on skin lesion area based on white color reference presents within-group residual error ΔE_{ab}^* ranging from 0.64 to 3.94. From Table 6, residual error on color stripes is significant and unpredictable comparing with the skin lesion color difference. Furthermore, there is no logical relationship between the color values of color stripes and that of skin

lesion. A color correction incorporating color stripe information and white reference tends to add more residual error on the skin lesion area.

Hence, given the experiment result of color correction with material and fabrication conditions, the proposed method based on white color reference generates the lowest residual error and presents stable performance under the same type of illumination.

In a more practical use condition, below factors may cause variability in color correction result:

- The use of different illumination type
- Camera automatic image processing
- The contamination of color reference surface on the fiducial marker

Given the scope of this thesis and limitation on fabrication, above sources of variability can be focus for future work. However, the efficacy of the proposed parametric and reference method is proven in reducing color distortion between images taken under the same type of illumination.

CHAPTER 4: CONCLUSION AND FUTURE WORK

Conclusion

A parametric method of imaging perspective alignment and color correction for skin lesion digital images is described.

For the perspective alignment, the estimation of perspective variation between two or more images is based on rigid features of a fiducial marker. With invariant features from fiducial points, the perspective variation is inferred and function parameters describing the transformation between two perspectives are calculated.

An inverse mapping based on the transformation function is applied on the pixel matrix of the target image such that the resulted image has the same imaging perspective as the reference image.

Under experimental conditions, the proposed approach is tested on 45 images taken from a variety of perspectives. After the perspective alignment, the resulted images of the same standard scene are at a comparable level with the uniform scaling, and perpendicular perspective. The experimental registration process of a standard view of the scene with the reference image gives residual error from 0 to 0.62% on the pixels of interest. Given a 95% confidence interval, the residual error is not significant and the variation is mainly caused by manual process of choosing control points.

Given the case of shifted fiducial marker location, the variation left is rotation which can be further approached by other image registration methods. B. McGregor's method using skin features is used to compensate for the rotation factor.

For the color correction, a mature color reference approach is used. Based on the diagonal model of color constancy, a color correction algorithm is proposed. The color correction algorithm estimates the effect of illumination on surface color of the object and then applies correction on the sensed image. The white patch of the fiducial marker is used for estimating illumination effect where the compensation value in the algorithm is based upon.

The color correction approach was tested on 60 images taken under illumination

conditions and imaging geometries. The proposed approach gives stable outputs for images taken under the same illumination type with a residual color difference of 0.64 to 3.94 in ΔE_{ab}^* value.

The low complexity of the algorithm and widely accepted principle make it suitable for color constancy in skin lesion imaging implementation.

In conclusion, the proposed parametric and fiducial approach of perspective alignment and color correction are suitable for skin lesion imaging in reducing perspective and color distortion.

Future Work

The study in this thesis was conducted with the intention of using and developing reliable and widely accepted approaches to achieve perspective uniformity and color constancy for skin lesion diagnostic purposes. Though the experiments gave significant insight into the efficacy of this method in maintaining constant measurement, the conditions of use simplified some factors which may have an effect on the performance in the field. All these factors should be further studied given the requirements of medical implementation.

Potential topics for future work:

Automation of the perspective alignment, skin lesion image registration and color correction processes. Based on the fiducial marker and automatic feature detection, the parameters for image registration and color correction can be generated automatically. One of the sources of variation left in the corrected images is the manual selection of fiducial points. In short, with a properly deigned automation, a higher level of accuracy and efficiency is expected.

Material choosing and fabrication on the fiducial marker are of importance since both geometric and color features are extracted from the surface of the marker. Rigid material is necessary. Surface flatness needs to be ensured. Given the fabrication of color reference of photography, knowledge can be acquired on material choosing and color printing on the fiducial white patch.

Given the planar surface assumption that the skin lesion and the attached fiducial marker are at a flat surface with little or no 3-D features, a well fabricated and small-size fiducial marker will make the assumption hold since the smaller the marker is, the more accurate it reflects the skin surface feature of the neighboring skin lesion. An experiment and statistical analysis are necessary to study above relationship and design.

This study has provided some insight on the efficacy of parametric method and fiducial approach for geometric alignment and color correction of digital skin lesion images. This is the first step towards constant measurement in skin lesion imaging. The majority of experiments are done under assumed conditions of use, and it is possible that the real use has different environmental factors and medical requirements. Given the context of medical implementation, an appropriate amount of clinical trial is necessary. By real-world assessment, further development of the methods and better clinical performance are expected.

REFERENCE

- [1] I. Maglogiannis, S. Pavlopoulos, & D. Koutsouris, (2004). "An Integrated Computer Supported Acquisition, Handling, and Characterization System for Pigmented Skin Lesions in Dermatological Images". IEEE Transactions on Information Technology in Biomedicine, VOL.9, No.1
- [2] G. Guillard & J M. Lagarde "Skin lesions segmentation and quantification from 3D body's models" Skin Research and Technology 2005; 11: 123–131
- [3] M. C. Gereli, N. Onsun, U. Atilganoglu,& C. Demirkesen, "Comparison of two dermoscopic techniques in the diagnosis of clinically atypical pigmented skin lesions and melanoma: seven-point and three-point checklists" International Journal of Dermatology 2010, 49, 33–38
- [4] M. Betke, H. Hong, D. Thomas, C. Prince, & J. P. Ko, "Landmark detection in the chest and registration of lung surfaces with an application to nodule registration" Medical Image Analysis 7 (2003) 265–281
- [5] B. Zitova & J. Flusser, "Image registration methods: a survey". ELSEVIER Image and Vision Computing 21 (2003) 977–1000
- [6] J. B. Antoine Maintz & Max A. Viergever. "A Survey of Medical Image Registration" Medical Image Analysis (1998) volume 2, number 1, page 1–37 Oxford University Press
- [7] Ed. Sonka and Milan (2000) "Handbook of medical imaging" SPIE--The International Society for Optical Engineering; 1 edition (June 15, 2000)
- [8] B. McGregor, Medical Imaging 1997. 25-28 February 1997, Newport Beach, California: Automatic algorithm for registering digital images of multiple skin lesions
- [9] G. Buchsbaum. "A spatial processor model for object colour perception". Journal of the Franklin Institute, 310, 1980
- [10] K. Barnard, L. Martin, A. Coath, & B. Funt (2002). "A comparison of computational color constancy algorithms-part I: methodology and experiments with synthesized data". IEEE Transactions on Image Processing, Vol.11, No.9

- [11]K. Barnard, L. Martin, A. Coath, & B. Funt (2002). “A comparison of computational color constancy algorithms-part II: experiments with image data”. IEEE Transactions on Image Processing, Vol.11, No.9
- [12]B. Funt & L. Shi (2010). “The effect of exposure on MaxRGB color constancy”. Human Vision and Electronic Imaging XV of SPIE-IS&T Electronic Imaging, SPIE Vol. 7527, 75270Y
- [13]C. C. Weng, H. Chen, & C. S. Fuh, (2005). A Novel Automatic White Balance Method for Digital Still Cameras
- [14]Help Menu of Matlab 7.11.0 (R2010b). Matlab Image Processing Toolbox. Matlab is a product of MathWorks
- [15]FUJIFILM XP20 Digital Camera Product Overview/Features/Specifications http://www.fujifilm.com/products/digital_cameras/xp/finepix_xp20/
- [16]C. Balas. “An imaging colorimeter for noncontact tissue color mapping”. IEEE Trans. Biomed. Eng., Vol 44, No. 6, 1993
- [17]C. R. Gonzalez, C. Rafael, Digital Image processing using MATLAB®
- [18]H. Y. Chong, S. J. Gortler, & T. Zickler. “The von Kries hypothesis and a basis for color constancy”. IEEE International Conference on Computer Vision 2007
- [19]Gray or White Card for Neutral Balancing http://www.rmimaging.com/information/gray_or_white.html
- [20]N. Pauler, “Paper Optics”. AB Lorentzen & Wettre, Sweden 1998.
- [21]M. Andersson & Ole Norberg. “Color measurements on prints containing fluorescent whitening agents”
- [22]G. Wyszecki and W. S. Stiles, Color Science, Concepts and Methods, Quantitative Data and Formulae. New York: Wiley, 1982.
- [23]M. Stokes, M.D. Fairchild, and R.S. Berns, “Precision requirements for digital color reproduction”, ACM Trans. Graphics, vol. 11, no. 4, pp. 406-422, 1992.
- [24]G.D. Finlayson, B.V. Funt & K. Barnard, “Color constancy under varying illumination” Computer Vision, 1995. Proceedings., Fifth International Conference on
- [25]G.D. Finlayson, “Color constancy in diagonal chromaticity space” Computer

- Vision, 1995. Proceedings., Fifth International Conference on
- [26]M. Andersson, “Digital Camera Calibration for Color Measurements on Prints”
Color Imaging XII: Processing, Hardcopy, and Applications, Reiner Eschbach;
Gabriel G. Marcu, Editors, 64930T, 2007
- [27]Ohlsson L & Federer R , “Efficient Use of Fluorescent Whitening Agents and
Shading Colorants in the Production of White Paper and Board”, TAPPSA
Technical Articles, <http://www.celuloseonline.com>, (2003)
- [28]T. J. Bruno, P. D. N. Svoronos. CRC Handbook of Fundamental Spectroscopic
Correlation Charts. CRC Press, 2005.

APPENDIX A

Matlab Source Code of Perspective Alignment

```
% read in the reference image, for example at location:
C:\Users\Desktop\fiducial.jpg

% call the input image "a"
a = imread('C:\Users\Desktop\fiducial.jpg');

% show the reference image "a"
imshow(a)

% read in the target image, for example at location:
C:\Users\Desktop\skinlesion.jpg

% call the input image "b"
b = imread('C:\Users\Desktop\skinlesion.jpg');

% Show the target image "b"
imshow(b)

% call the "Control Point Selection Tool" to obtain the geometric location of 4 pairs of
fiducials in two images

% Manually select 4 pairs of corresponding control points in two images
% In the Control Point Selection Tool, click the File menu and choose the Export Points
to Workspace option and the geometric location of each 4 control points in two images
are recorded as "input_points" and "base_points"
cpselect(a, b)

% calculate 2-D spatial transformation function parameters
% "input_points" and "base_points" are input values
% the perspective variation is caused by camera perspective and the skin surface variation
can be ignored in this case of variation correction
% "projective" is chosen as the transformation type
mytform = cp2tform(input_points, base_points, 'projective');

% with the transformation function which transform the reference image to the target
image, a reverse mapping is applied on the target image such that the registered image has
```

the same perspective with the reference image

% fill the empty area after the transformation with white color and display the registered

image

```
registered = imtransform(a, mytform,...'FillValues', 255);
```

```
imshow(registered);
```

APPENDIX B

Matlab Source Code of Color Correction

```
% input jpg format image of the cropped white patch
% input jpg format image of the skin lesion
% input image data with double-precision floating-point real-world value
input_imp=double(imread('C:\Users\Desktop\whitepatch.jpg'));
input_im=double(imread('C:\Users\Desktop\skinlesion.jpg'));
% show the input image as 28 (255) per color channel
% call the image “input image”
imshow(uint8(input_im));
title('input image');

% apply the “color reference-based White Patch” function, with white
patch image and skin lesion image as input

% call for R, G, and B channel gain values and the corrected image of the
skin lesion

% call the output image “Corrected”

[Rgain,Ggain,Bgain,output_data]=White_Patch(input_imp,input_im);
figure;imshow(uint8(output_data));
title('Corrected');

% the coding of the function

function[Rgain,Ggain,Bgain,output_data]=White_Patch(input_imp,input_i
m)
R=input_imp(:,:,1);
G=input_imp(:,:,2);
B=input_imp(:,:,3);
Rav=mean(mean(R));
Gav=mean(mean(G));
Bav=mean(mean(B));
Rgain=255/Rav;
Ggain=255/Gav;
Bgain=255/Bav;

output_data(:,:,1)=input_im(:,:,1)*Rgain;
output_data(:,:,2)=input_im(:,:,2)*Ggain;
output_data(:,:,3)=input_im(:,:,3)*Bgain;
```

APPENDIX C

Matlab Source Code of Image Segmentation

```
% read in the reference image, for example at location:
C:\Users\Desktop\skinlesion.jpg

I = imread('C:\Users\Desktop\skinlesion.jpg');

% a blur or smoothing is used to reduce image noise. Most edge-detection
algorithms are sensitive to noise. Using blur filter before edge detection aims to
reduce the sensitivity to noisy environment which improves the result of the following
edge-detection algorithm.
% simple averaging filter
% set lower and upper limits
% input array values outside the bounds of the array are computed by
mirror-reflecting the array across the array border.
u=25;

l=35;

k=u*l;

h = ones(u,l) / k;

II = imfilter(I,h,'symmetric');

% display the original image and the filtered image in subplots
figure

subplot(2,2,1),imshow(I), title('Original image');

subplot(2,2,2), imshow(II), title('Filtered Image');

% convert the RGB filtered image into gray level image
IG=rgb2gray(II);

% stretchlim(IG) returns LOW_HIGH, a two-element vector of pixel values that
specify lower and upper limits that can be used for contrast stretching image IG. By
default, values in LOW_HIGH specify the bottom 1% and the top 1% of all pixel
values. The gray values returned is then used by the imadjust function to increase the
contrast of an image.

III = imadjust(IG,stretchlim(IG),[]);

% level = graythresh(I) computes a threshold (level) that can be used to convert an
intensity image to a binary image with im2bw. level is a normalized intensity value
that lies in the range [0, 1].
```

% The `graythresh` function uses Otsu's method, which chooses the threshold to minimize the intraclass variance of the black and white pixels.[1] Otsu, N., "A Threshold Selection Method from Gray-Level Histograms," *IEEE Transactions on Systems, Man, and Cybernetics*, Vol. 9, No. 1, 1979, pp. 62-66.

```
level = graythresh(III);

% Convert image to binary image, based on gray level threshold above
% BWJ = im2bw(III, level) converts the grayscale image I to a binary image. The
output image BWJ replaces all pixels in the input image with luminance greater than
level with the value 1 (white) and replaces all other pixels with the value 0 (black).
BWJ = im2bw(III, level);

% d = size(M) returns the number of key-value pairs in dimensions 1 and 2 of map M. Output d
is a two-element row vector [n,1], where n is the number of key-value pairs. dim =
size(BWJ)

% ones - Create array of all ones, call the array IN
IN=ones(dim(1),dim(2));

% C = xor(A, B) performs an exclusive OR operation on the corresponding elements
of arrays A and B. The resulting element C(i,j,...) is logical true (1) if A(i,j,...)
or B(i,j,...), but not both, is nonzero.
% the BW is a matrix of 0 and 1 as element values. The segmented skin lesion area
location is all one.
BW=xor(BWJ, IN);

% show the BW matrix as black and white image
subplot(2,2,3), imshow(BW), title('Black and White');

% input RGB skin lesion image
% call it "A"
A = imread('C:\Users \Desktop\skinlesion.jpg');

% use the binary black and white image matrix as image filer, and multiply the R, G and
B channels with the binary matrix, call the resulted matrix CR, CG and CB
CR=BW*(A(:, :, 1));
CG=BW*(A(:, :, 2));
CB=BW*(A(:, :, 3));

% combine the filtered matrix of R, G and B value; get the segmented skin lesion image
C=CR+CG+CB;
imshow(C)

% the Performance Metrics of Color Correction is to be continued in Appendix D using
binary image BW and skin lesion image A
```

APPENDIX D

Performance Metrics of Color Correction: RGB Values

```
% continue with the sample image in Appendix C
% call red channel matrix of the segmented skin lesion image RI
RI = I(:, :, 1)
Imshow(RI)
% multiple all matrix elements in binary matrix pair-wisely with R channel matrix;
note: the red channel value is successfully segmented.
RJ=immultiply(BW,RI)
Imshow(J)
% the average R channel value and std dev across all pixel counts are calculated; the
calculation is done on all non-zero elements
Ravg = mean(nonzeros(RJ));
Rstd = std2(nonzeros(RJ))
% repeat on other two channels for average and standard deviation values
```

APPENDIX E

Performance Metrics of Color Correction: CIE Lab Color

Difference

```
% concatenate the 2-d matrices along the 3rd dimension; show the new image in
sRGB format
RGBNEW = cat(3, RJ, GJ, BJ);
imshow(RGBNEW)
% transform the sRGB image into CIElab format
cform = makecform('srgb2lab');
lab = applycform(RGBNEW,cform);
% rename the L*, a* and b* channels
l = lab(:,:,1);
a = lab(:,:,2);
b = lab(:,:,3);
% segment the lesion area of interest by multiply the three channels with binary mask
BW.
ls=immultiply(BW,l)
as=immultiply(BW,a)
bs=immultiply(BW,b)
% calculate the average values of the L*, a*, and b* channels
lavg = mean(nonzeros(ls));
aavg = mean(nonzeros(as));
bavg = mean(nonzeros(bs));
% the mean values of L*, a*, and b* channels of a group images are calculated and
used as standard value; the mean values of L*, a*, and b* channels of each image are
used as sample values.
```

The ΔL^* , Δa^* , and Δb^* are from the subtraction of sample values from standard values.

The color difference is calculated using the formula below:

$$\Delta E_{ab}^* = \sqrt{(\Delta L^{*2} + \Delta a^{*2} + \Delta b^{*2})}$$

APPENDIX F

Performance Metric of Perspective Alignment

```
% input target and reference images
a = imread('C:\Users\Desktop\target.jpg');
b = imread('C:\Users\Desktop\reference.jpg');
% choose control points and register the target image matrices a
cpselect(a, b)
mytform = cp2tform(input_points, base_points, 'projective');
registered = imtransform(a, mytform);
% align the registered image a with the reference image b, convert image a into the
size of image b
registered1 = imtransform(a,mytform,...
                        'FillValues', 150,...
                        'XData', [1 size(b,2)],...
                        'YData', [1 size(b,1)]);

% calculate the absolute difference between image matrices of a and b. result in a
three channel matrices Z
Z = imabsdiff(b, registered1)
% threshold and filter the three channel image matrices by a brightness value of 0.3
(range from 0-1), result in a binary image BW
BW = im2bw(Z, 0.3)
% count the number of nonzero elements in matrix BW and calculated the ratio of
nonzero elements over all pixel count in BW
% show binary image BW as residual error description
% show the registered image
n1= nnz(BW)/prod(size(BW))
nnz(BW)
figure, imshow(BW)
figure, imshow(registered1)
```